

University of Windsor

## Scholarship at UWindor

---

Electronic Theses and Dissertations

Theses, Dissertations, and Major Papers

---

1982

### Analysis of developing region of a submerged laminar free jet.

Mylvaganam. Arulraja  
*University of Windsor*

Follow this and additional works at: <https://scholar.uwindsor.ca/etd>

---

#### Recommended Citation

Arulraja, Mylvaganam., "Analysis of developing region of a submerged laminar free jet." (1982). *Electronic Theses and Dissertations*. 1165.

<https://scholar.uwindsor.ca/etd/1165>

This online database contains the full-text of PhD dissertations and Masters' theses of University of Windsor students from 1954 forward. These documents are made available for personal study and research purposes only, in accordance with the Canadian Copyright Act and the Creative Commons license—CC BY-NC-ND (Attribution, Non-Commercial, No Derivative Works). Under this license, works must always be attributed to the copyright holder (original author), cannot be used for any commercial purposes, and may not be altered. Any other use would require the permission of the copyright holder. Students may inquire about withdrawing their dissertation and/or thesis from this database. For additional inquiries, please contact the repository administrator via email ([scholarship@uwindsor.ca](mailto:scholarship@uwindsor.ca)) or by telephone at 519-253-3000ext. 3208.

CANADIAN THESES ON MICROFICHE

I.S.B.N.

THÈSES CANADIENNES SUR MICROFICHE



National Library of Canada  
Collections Development Branch

Canadian Theses on  
Microfiche Service

Ottawa, Canada  
K1A 0N4

Bibliothèque nationale du Canada  
Direction du développement des collections

Service des thèses canadiennes  
sur microfiche

NOTICE

The quality of this microfiche is heavily dependent upon the quality of the original thesis submitted for microfilming. Every effort has been made to ensure the highest quality of reproduction possible.

If pages are missing, contact the university which granted the degree.

Some pages may have indistinct print especially if the original pages were typed with a poor typewriter ribbon or if the university sent us a poor photocopy.

Previously copyrighted materials (journal articles, published tests, etc.) are not filmed.

Reproduction in full or in part of this film is governed by the Canadian Copyright Act, R.S.C. 1970, c. C-30. Please read the authorization forms which accompany this thesis.

THIS DISSERTATION  
HAS BEEN MICROFILMED  
EXACTLY AS RECEIVED

AVIS

La qualité de cette microfiche dépend grandement de la qualité de la thèse soumise au microfilmage. Nous avons tout fait pour assurer une qualité supérieure de reproduction.

S'il manque des pages, veuillez communiquer avec l'université qui a conféré le grade.

La qualité d'impression de certaines pages peut laisser à désirer, surtout si les pages originales ont été dactylographiées à l'aide d'un ruban usé ou si l'université nous a fait parvenir une photocopie de mauvaise qualité.

Les documents qui font déjà l'objet d'un droit d'auteur (articles de revue, examens publiés, etc.) ne sont pas microfilmés.

La reproduction, même partielle, de ce microfilm est soumise à la Loi canadienne sur le droit d'auteur, SRC 1970, c. C-30. Veuillez prendre connaissance des formules d'autorisation qui accompagnent cette thèse.

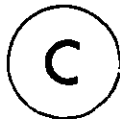
LA THÈSE A ÉTÉ  
MICROFILMÉE TELLE QUE  
NOUS L'AVONS RECUE

ANALYSIS OF DEVELOPING REGION OF A  
SUBMERGED LAMINAR FREE JET

A THESIS

Submitted to the Faculty of Graduate Studies through  
the Department of Mechanical Engineering in Partial  
Fulfillment of the Requirements for the Degree of  
Master of Applied Science at the  
University of Windsor

by



Mylvaganam Arulraja

Windsor, Ontario, Canada

1982

© Mylvaganam Arulraja 1982

**774689**

## ABSTRACT

An implicit finite difference method is used to obtain a numerical solution of an incompressible axisymmetric submerged laminar free jet issuing from a long tube. Based on the results of the finite difference method the velocity profile in the developing region is modelled by combining a parabolic velocity profile and a radially shifted Schlichting velocity profile. A simplified derivation of the axial velocity variation along the jet centre line is also presented. The axial centre line velocities and their first derivatives are matched at the boundary of the developing and developed flow region in order to determine the virtual origin and the developing length of the jet. These results exhibit reasonable agreement with the existing experimental and analytical results.

## ACKNOWLEDGEMENTS

The writer expresses gratitude to Drs. K. Sridhar and G.W. Rankin for their stimulating encouragement and guidance in the preparation of the work, to Mrs. B. Carr for the typing of the thesis, and to the Natural Sciences and Engineering Research Council of Canada for its financial support through grant number A-2190.

## TABLE OF CONTENTS

	Page
ABSTRACT	iii
ACKNOWLEDGEMENTS	iv
TABLE OF CONTENTS	v
LIST OF FIGURES	vii
LIST OF TABLES	ix
NOMENCLATURE	x
CHAPTER I INTRODUCTION	1
1.1 Aims	2
CHAPTER II LITERATURE SURVEY	3
2.1 Jets Originating from an Infinitesimal Orifice	3
2.2 Jet with a Parabolic Exit Velocity Profile	5
2.2.1 Theoretical Studies	5
2.2.2 Experimental Studies	9
CHAPTER III ANALYSIS OF DEVELOPING REGION OF A SUBMERGED LAMINAR FREE JET	12
3.1 Introduction	12
3.2 Theoretical Analysis	12
3.3 Numerical Computation	16
3.4 Analysis of the Finite Difference Solution	17
3.4.1 Schlichting Velocity Profile in the Free Shear Layer	18
3.5 Simplified Derivation of the Maximum Velocity Decay	19
3.5.1 Variation of Maximum Velocity with Axial Distance	20

3.5.2	Matching of Maximum Velocity Variations	23
CHAPTER IV	RESULTS AND DISCUSSION	25
4.1	Finite Difference Solution	25
4.1.1	Centre Line Velocity Variation	25
4.1.2	Parabolic Core of the Jet	26
4.1.3	Jet Half-Radius	27
4.1.4	Axial Velocity Profiles	28
4.2	Velocity Model in the Developing Region	28
4.3	Simplified Derivation of the Variation of Axial Velocity	29
CHAPTER V	CONCLUSIONS	33
5.1	Finite Difference Solution	33
5.2	Simplified Derivation of Maximum Velocity Decay	33
REFERENCES		35
FIGURES		37
TABLES		59
APPENDICES		62
A	MAIN COMPUTER PROGRAM	62
B	UNCERTAINTY ANALYSIS	76
C	NLIN COMPUTER PROGRAM	77
D	ADDITIONAL MODIFICATION IN PAI AND HSIEH'S COMPUTER PROGRAM	79
VITA AUCTORIS		80



## LIST OF FIGURES

Figure	Title	Page
1	Velocity Profile Model	37
2	Finite Difference Grid	38
3	Experimental Centre Line Velocity Decay	39
4	Analytical Centre Line Velocity Decay	40
5	Variation of Parabolic Core Width	41
6	Jet Growth	42
7	Velocity Variation at Different Radial Locations	43
8	Variation of Schlichting Parameter $X_{cv}$	44
9	Variation of Schlichting Parameter $\frac{Y}{Re_c}$	45
10	Variation of Schlichting Parameter A	46
11	Comparison of Velocity Profile Model and Finite Difference Solution ( $X_c = 0.001$ )	47
12	Comparison of Velocity Profile Model and Finite Difference Solution ( $X_c = 0.004$ )	48
13	Comparison of Velocity Profile Model and Finite Difference Solution ( $X_c = 0.008$ )	49
14	Comparison of Velocity Profile Model and Finite Difference Solution ( $X_c = 0.016$ )	50
15	Comparison of Velocity Profile Model and Finite Difference Solution ( $X_c = 0.028$ )	51
16	Comparison of Velocity Profile Model and Finite Difference Solution ( $X_c = 0.04$ )	52
17	Comparison of Velocity Profile Model and Finite Difference Solution ( $X_c = 0.048$ )	53
18	Comparison of Velocity Profile Model and Finite Difference Solution ( $X_c = 0.056$ )	54

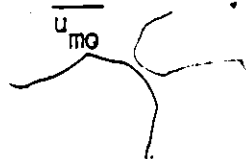
Figure	Title	Page
19	Comparison of Velocity Profile Model and Finite Difference Solution ( $X_c = 0.1$ )	55
20	Maximum Velocity Decay	56
21	Comparison of Matching Schemes	57
22	Solution Domain of the Jet	58

## LIST OF TABLES

Table	Title
1.	Axial Velocity Distribution.
2.	Development Lengths and Virtual Origin Locations.
3.	Schlichting Parameters in the Free Shear Layer.

## NOMENCLATURE

A	nondimensional radial shift of the Schlichting profile defined in Figure 1; constant in equation (2.4)
a	radius of the nozzle
J	momentum flux
N	number of grid points in the radial direction
p	pressure
r	radial distance
$r_{m/2}$	radial distance from the axis of the jet to a location where $u = 0.5 u_m$
$r_p$	width of the parabolic core
R	nondimensional radial distance, $\frac{r}{a}$
$R_{m/2}$	$r_{m/2}/a$
$R_p$	nondimensional width of the parabolic core, $\frac{r_p}{a}$
$Re_c$	Reynolds number, based on the centre line velocity at the nozzle exit, $\frac{u_{m0} a}{\nu}$
u	$u(x,r)$ = axial velocity component
$u(0,0)$	centre line velocity of the nozzle exit
$u_r$	radial velocity component in spherical coordinates
$u_\theta$	azimuthal velocity component in spherical coordinates
$u_{m0}$	$u(0,0)$
$u_m$	$u(x,0)$
$u(x,0)$	centre line velocity along the axis of the jet
U	$\frac{u}{u_m}$
$U_m$	$\frac{u_m}{u_{m0}}$



$U_0$	$\frac{u(x,r)}{u_{mo}}$
$U_{FIN}$	U obtained from finite difference technique
$U_{MOD}$	U obtained from velocity model
$v$	radial component of velocity
$\nu$	$\frac{\rho \nu a}{\mu}$
$x$	axial distance measured from nozzle exit plane
$x_s$	axial distance measured from point source
$x_v$	axial distance from point source to the nozzle exit
$x_l$	developing length of the jet measured from the nozzle exit
$x_c$	$\frac{x}{a Re_c}$
$x_{cl}$	nondimensional developing length of the jet, $\frac{x_l}{a Re_c}$
$x_{cv}$	nondimensional axial distance to the virtual origin, $\frac{x_v}{a Re_c}$
$\xi$	similarity variable defined in equation (2.3)
$\mu$	dynamic viscosity
$\rho$	density
$\nu$	kinematic viscosity
$\theta$	spherical coordinate
$\alpha$	defined in equation (2.9)
$\gamma$	Schlichting's jet spread parameter

## CHAPTER I

### INTRODUCTION

When a fluid exits from a supply tube into an unbounded medium of the same fluid it is called a submerged free jet. Downstream of the exit, the jet entrains fluid from the surroundings. Depending upon the Reynolds number, the jet could be either laminar or turbulent. This thesis is concerned with laminar jets only.

Submerged free jets can be divided into a developing and developed region. The developing region is one near the tube exit and velocity profiles in this region are nonsimilar. The velocity profiles are similar in the developed region. The velocity profiles in the developing region are determined by the exit velocity profile of the jet which depends on the length of the supply tube. If the supply tube is very short almost a uniform velocity profile is obtained since the wall layer growth is negligible. In this case the developing region is identified by the existence of a potential core and an annular free shear layer. The centre line velocity of the jet remains constant in the potential core. The jet becomes fully developed at a distance from the exit called the developing length. The radius of the potential core reduces to zero at this distance and the centre line velocity begins to decay in the developed region.

If the supply tube is sufficiently long, the flow inside the tube becomes fully developed and this results in a parabolic velocity profile at the exit. In this case the developing region is identified by a parabolic core where the exit parabolic velocity profile persists, however, with a decreasing centre line velocity and an annular free-shear layer.

It is also possible to obtain a partly parabolic and partly uniform velocity profile at the exit by varying the length of the tube. This case is not considered in this thesis.

This thesis is devoted to the study of the developing region of a submerged axisymmetric laminar free jet with parabolic exit velocity profile. The present analysis has application in the design of fluidic devices such as turbulence amplifiers.

### 1.1 Aims

The purpose of the present work comprises of the following:

- (1) To present, in a tabular form, a finite difference solution of the boundary layer equations for the case of an axisymmetric jet issuing from a tube, with a parabolic exit velocity profile, into an infinite expanse of fluid.
- (2) Analyse the results for the developing jet to determine the region where the velocity profile is parabolic to a good approximation.
- (3) To obtain a velocity profile model in the free shear layer by modifying the Schlichting velocity profile with its axis shifted radially and using suitable length and velocity scales.
- (4) To present a simplified derivation of the centre line velocity variation and to determine the developing length and virtual origin.

CHAPTER II  
LITERATURE SURVEY

The developing and developed regions of axisymmetric laminar free jets have been analysed theoretically and experimentally. The investigations can be grouped into three sections depending upon the initial condition of the jet:

- (1) Jet originating from an infinitesimal orifice.
- (2) Jet with a parabolic exit velocity profile.
- (3) Jet with a uniform exit velocity profile.

This survey is limited to the first two cases.

2.1 Jet Originating from an Infinitesimal Orifice

The exact solution for velocity profiles of a free jet was obtained by Schlichting [14]. He solved the momentum equation in the axial direction under the usual boundary layer simplifications, and the continuity equation along with the following assumptions:

1. The jet originates from a point source with infinite velocity.
2. The pressure is constant hence the momentum flux is constant in the axial direction.
3. The velocity profiles are similar.

The expressions for the axial and radial velocities are of the following form:

$$u = \frac{3}{8\pi} \frac{J}{u x_s} \frac{1}{\left(1 + \frac{\xi^2}{4}\right)^2} \quad (2.1)$$



and

$$v = \frac{1}{4} \sqrt{\frac{3J}{\pi\rho}} \frac{1}{x_s} \frac{\xi - \frac{\xi^3}{4}}{\left(1 + \frac{1}{4} \xi^2\right)^2} \quad (2.2)$$

where

$$\xi = \sqrt{\frac{3J}{16\pi\rho}} \frac{1}{v} \frac{r}{x_s} \quad (2.3)$$

Since it is assumed that the jet originates from a point, Schlichting's solutions are applicable only far downstream of the exit for a jet issuing from an orifice of finite size.

Landau [9] determined the velocity profiles accurately for arbitrary Reynolds numbers by a rigorous solution of Navier-Stokes equations. He employed spherical co-ordinates in his analysis and determined the pressure field of the jet. The distribution of the pressure is given by:

$$p = \frac{4\rho v^2}{r^2} \frac{(A \cos\theta - 1)}{(A - \cos\theta)^2} \quad (2.4)$$

where the constant A is related to the momentum of the jet. For large angles the velocities are given by:

$$u_\theta = -2v \frac{\cot \frac{\theta}{2}}{r} \quad (2.5)$$

and

$$u_r = -2 \frac{v}{r} \quad (2.6)$$

For small angles the velocities are given by:

$$u_{\theta} = - \frac{4v\theta}{\alpha^2 + \theta^2} \quad (2.7)$$

and

$$u_r = 8v \frac{\alpha^2}{(\alpha^2 + \theta^2)^2} \quad (2.8)$$

where

$$\alpha = \frac{32\pi v^2 \rho}{3J} \quad (2.9)$$

The conditions for the case of small angles are in accordance with the results obtained by Schlichting.

Landau's solutions can be applied only in a region far downstream of the point source.

Rumer [13] showed that Landau's solution technique gives zero mass flowrate at the origin. To obtain a finite flowrate he included two function components in the expressions for the velocities and the pressure. From Landau's and Rumer's results it can be concluded that the addition of higher order terms in their previously mentioned expansions would yield better solutions at the expense of the labour involved in obtaining them.

## 2.2 Jet with a Parabolic Exit Velocity Profile

### 2.2.1 Theoretical Studies

Andrade and Tsien [2] introduced the virtual origin technique to obtain the velocity profiles for a jet issuing from an orifice of

finite size. They assumed that the jet originated from a point inside the supply tube and obtained an expression for the kinetic energy of the fluid at the tube exit using Schlichting's velocity profile. They also obtained another expression for the kinetic energy using parabolic velocity profile at the exit.

Equating these two expressions they obtained an approximate value for the virtual origin given by the equation:

$$\frac{x_v}{a} = 0.1 Re_c \quad (2.10)$$

Schlichting's expression for the axial velocity with modified axial distance is given by:

$$u = \frac{3}{8\pi} \frac{J}{\mu(x + x_v)} \frac{1}{\left(1 + \frac{x^2}{4}\right)} \quad (2.11)$$

The solution of Andrade and Tsien can be applied only in the developed region of the jet since they have used a point source flow model.

Other investigators have determined other approximations of the location of the virtual origin by matching flow quantities such as centre line velocity and mass flowrate at the nozzle exit as described by Bell [4,5].

Dmitriev and Kulesova [7] compared their theoretical investigations and experimental measurements. A total pressure probe was used to measure velocity in their experiment. They employed two different versions of Schlichting's expression to represent the

velocity profiles in the near region of the exit and far downstream of the exit where the latter is the same as that used by Andrade and Tsien. The flow model in its general form is given by:

$$u = \frac{u_m}{(1 + Br^2)^2} \quad (2.12)$$

In the near region of the jet exit  $u_m$  and  $B$  are given by the following equations:

$$\frac{u_m}{u_{m0}} = 1 - \frac{4x}{aRe_c} \quad (2.13)$$

and

$$B = U_m^2 \quad (2.14)$$

The centre line velocities of the developing region and the developed region were matched to obtain the developing length. The real part of a complex root of the resulting quadratic equation was chosen as the developing length and it was found to be:

$$\frac{x_d}{a} = 0.0752 Re_c \quad (2.15)$$

Their variation of centre line velocity with the axial distance has a discontinuity at the boundary of the developing and fully developed regions.

Rankin [12] obtained an approximate solution to the velocity

distribution by an integral method. The velocity profile assumed, reduces to a parabola at the exit however far downstream of the jet exit it reduces only to a "near" Schlichting profile. He also obtained an equation for the centreline velocity decay. Rankin's theoretical investigations show better agreement with his experimental results near the jet exit.

Pai and Hsieh [10,11] employed an implicit finite difference technique to solve the simplified boundary layer equations. They graphically presented the velocity profiles, centre line velocity decay and the spread of the jet. The spread of the jet determined by Pai and Hsieh is in disagreement with that of Rankin [12].

du Plessis et al [8] solved the momentum and the continuity equations in the Von Mises plane. They employed an explicit algorithm and in order to keep the algorithm in the recurrence relationship the velocity was expressed as a Fourier cosine series which has the characteristic of vanishing gradients at the axis of symmetry. They compared their numerical results with their own experimental values.

Tsang [16] employed a three point, implicit finite difference scheme. This method has a higher order of truncation error in comparison to Pai and Hsieh's implicit representation and explicit representation of du Plessis et al and it needs initial conditions at two consecutive axial locations to start the computation. Tsang produced the results for the turbulent and the laminar jet.

### 2.2.2 Experimental Studies

Andrade and Tsien [2] employed a suspended particle technique to measure the velocity profiles in the fully developed region. The experimental velocity profiles are in good agreement with a modified form of Schlichting's velocity profiles suggested by them.

Symons et al. [15] investigated a helium into helium jet issuing from a vertical tube of 0.254 centimeters in diameter with fully developed flow at the exit of the tube. A total pressure probe which had a circular opening of 0.015 centimeter diameter was used to take the measurements. They measured the velocity profiles and the centre line velocity decay at Reynolds numbers ( $Re_c$ ) of 437 and 1839 at 0, 3, 6, 10, 15 and 25 diameters from the tube exit. They also measured the spread of the jet to be  $2^\circ$  to  $3^\circ$  for the Reynolds numbers of 437, 925, and 1839 and reported that the magnitude of the spread angle did not significantly depend upon Reynolds numbers investigated. They predicted that the behaviour of the developing region of the jet to be dependent on the initial velocity profile of the jet.

Chang [6] made an analytical and experimental study of a laminar free jet with parabolic exit velocity profile. An aqueous solution of resin (polyox WSR N-3000, Union Carbide product) was used as the fluid medium. The measurements were taken with a Constant-Temperature Anemometer. He graphically presented his experimental velocity profiles for different axial locations and for Reynolds numbers of 430 and 600. Based on the experimental data he

derived an expression for the velocity distribution in the developing zone and obtained an equation for the location of the virtual origin.

du Plessis et al [8] numerically and experimentally investigated an oil-to-oil laminar free jet. A hot-film probe was used for the measurement of velocities. Their algorithm agreed well with their experimental results in the developing region of the jet. They also showed that the velocity profiles obtained from the modified Schlichting's expression suggested by Andrade and Tsien did not compare well in the developing region.

Abramovich and Solan [1] obtained an empirical correlation for the centre line velocity decay as follows:

$$U_m = \frac{1}{c x^* + b} \quad \text{for } x^* > 0.2 \quad (2.16)$$

where

$$x^* = \frac{x}{2a \sqrt{Re_c}}$$

and  $c = 1.13$  with  $b = 0.89$ .

The authors claim that their results are in good agreement with Andrade and Tsien's results in the scaling of  $x^*$ . However, it should be noted that the nondimensional form of boundary layer equations yield  $\frac{x}{aRe_c}$  as the nondimensional axial distance.

Rankin [12] in his experimental investigation used a Laser Doppler Anemometer in dual beam mode. He presented the axial velocity profiles, the variation of centre line velocity, developing length of

the jet and the location of the virtual origin. His theoretical and experimental results are in good agreement. Since a Laser Doppler Anemometer does not provide any physical disturbance to the fluid flow unlike a pressure probe or a hot-film probe the results obtained by Rankin [12] are more accurate than the results obtained by the other investigators. Rankin has experimentally verified that a parabolic core exists in the developing region of the jet.

The above literature survey reveals that

- (i) no attempt has, as yet, been made to model the free shear layer with a modified form of Schlichting's expression in the developing region.
- (ii) the developing length and the position of the virtual origin have not been well defined theoretically.

Solutions to the problems mentioned above are presented in this thesis.



## CHAPTER III

### ANALYSIS OF DEVELOPING REGION OF A

### SUBMERGED LAMINAR FREE JET

#### 3.1 Introduction

In this chapter the numerical solution of an incompressible laminar free jet issuing from a long tube is presented in tabular form. The results are analysed to verify the experimental prediction [8] which indicates the existence of a parabolic core in the developing region. Based on this fact, a simplified derivation of the centre line velocity has been obtained. Further, the length of the developing region and the location of the virtual origin have been obtained by matching the centre line velocity variations at the boundary of the developing and fully developed regions. The velocity profile in the annular free shear layer of the developing region is modelled by shifting the centre of the Schlichting velocity profile (Figure 1). The present solution is compared with existing experimental and analytical results. The variation of Schlichting parameters, namely,  $x_v$ ,  $\frac{\gamma}{Re_c}$  and  $A$  are also obtained in the developing region.

#### 3.2 Theoretical Analysis

The equations of motion for a steady, axisymmetric laminar jet of an incompressible fluid may be written as follows:

$$\frac{\partial u}{\partial x} + \frac{\partial v}{\partial r} + \frac{v}{r} = 0 \quad (3.1)$$

$$u \frac{\partial u}{\partial x} + v \frac{\partial u}{\partial r} = \nu \left( \frac{1}{r} \frac{\partial u}{\partial r} + \frac{\partial^2 u}{\partial r^2} \right) \quad (3.2)$$

The non dimensional form of the equations, (3.1) and (3.2), can be written as follows:

$$\frac{\partial U_0}{\partial X_c} + \frac{\partial V}{\partial R} + \frac{V}{R} = 0 \quad (3.3)$$

$$U_0 \frac{\partial U_0}{\partial X_c} + V \frac{\partial U_0}{\partial R} = \frac{1}{R} \frac{\partial U_0}{\partial R} + \frac{\partial^2 U_0}{\partial R^2} \quad (3.4)$$

where

$$U_0 = \frac{u}{u_{mo}}, \quad V = \frac{vpa}{\mu}, \quad R = \frac{r}{a}, \quad (3.5)$$

$$X_c = \frac{x}{aRe_c} \quad \text{and} \quad Re_c = \frac{\rho a u_{mo}}{\mu}$$

The initial and boundary conditions are:

$$\begin{aligned} X_c = 0 \text{ and } R < 1: U_0 &= 1 - R^2 \\ X_c = 0 \text{ and } R > 1: U_0 &= 0 \\ X_c > 0: V &= 0 \text{ at } R = 0 \\ U_0 &= 0 \text{ at } R \rightarrow \infty \end{aligned} \quad (3.6)$$

At the axis of symmetry,

$$\text{Limit}_{R \rightarrow 0} \frac{V}{R} = \frac{\partial V}{\partial R} \quad \text{and} \quad \text{Limit}_{R \rightarrow 0} \frac{1}{R} \frac{\partial U_0}{\partial R} = \frac{\partial^2 U_0}{\partial R^2}$$

Therefore the continuity and the momentum equations at the axis of symmetry can be written as follows:

$$\frac{\partial U_m}{\partial X_c} + 2 \frac{\partial V}{\partial R} = 0 \quad (3.7)$$

$$U_m \frac{\partial U_m}{\partial X_c} = 2 \frac{\partial^2 U_o}{\partial R^2} \quad (3.8)$$

Since there are restrictions to small mesh sizes in the explicit finite difference scheme due to stability criteria and the implicit scheme is universally stable for all mesh sizes the latter is chosen to solve the partial differential equations (3.3) and (3.4).

Figure [2] shows the grid imposed on the flow field. Backward finite difference representations are used to replace the partial derivatives in the axial direction and central difference representations are used to replace the partial derivatives in the radial direction.

The representations used at a point  $(j+1, k)$  are:

$$\left. \begin{aligned} U_o \frac{\partial U_o}{\partial X_c} &= U_{o,j,k} \left[ \frac{U_{o,j+1,k} - U_{o,j,k}}{\Delta X} \right] \\ v \frac{\partial U_o}{\partial R} &= v_{j,k} \left[ \frac{U_{o,j+1,k+1} - U_{o,j+1,k-1}}{2(\Delta R)} \right] \\ \frac{1}{R} \frac{\partial U_o}{\partial R} &= \frac{1}{R_k} \left[ \frac{U_{o,j+1,k+1} - U_{o,j+1,k-1}}{2(\Delta R)} \right] \\ \frac{\partial^2 U_o}{\partial R^2} &= \frac{U_{o,j+1,k+1} - 2U_{o,j+1,k} + U_{o,j+1,k-1}}{(\Delta R)^2} \end{aligned} \right\} \quad (3.9)$$

Using these representations, equations (3.4) and (3.7) may be written in the following finite difference form:

$$\begin{aligned}
& \left[ \frac{1}{2R_K(\Delta R)} - \frac{V}{2(\Delta R)} - \frac{1}{(\Delta R)^2} \right] U_{o_{j+1,k-1}} \\
& + \left[ \frac{2}{(\Delta R)^2} + \frac{U_o}{\Delta X} \right] U_{o_{j+1,k}} \\
& + \left[ \frac{1}{2\Delta R} - \frac{1}{(\Delta R)^2} - \frac{1}{2R_K(\Delta R)} \right] U_{o_{j+1,k+1}} \\
& = \frac{U_o U_{o_{j,k}}}{\Delta X}
\end{aligned} \tag{3.10}$$

and

$$\left( \frac{U_o}{\Delta X} + \frac{4}{(\Delta R)^2} \right) U_{o_{j+1,k}} - \frac{4}{(\Delta R)^2} U_{o_{j+1,k-1}} = \frac{U_o}{\Delta X} U_{o_{j,k}} \tag{3.11}$$

(N-1) number of simultaneous equations are obtained by applying the momentum equation in the forms given by equations (3.10) and (3.11) at each node along the radial direction at a particular axial location where N is the number of grid points considered in the radial direction. These simultaneous equations are solved for the axial velocities by Thomas' algorithm described in references 10 and 11.

The continuity equation may be written in integro-differential form as follows:

$$V = -\frac{1}{R} \int_0^R \left( \frac{\partial U_o}{\partial X_c} \right) R dR \tag{3.12}$$

Using the trapezoidal rule the equation (3.12) may be written in the finite difference form:

$$V_{j+1,k} = V_{j+1,k-1} - \frac{\Delta R}{2R_K} \left[ \frac{R_{K+1} U_{0,j+1,K} - R_K U_{0,j,K}}{\Delta X} + \frac{R_{K-1} U_{0,j+1,K-1} - R_{K-1} U_{0,j,K-1}}{\Delta X} \right] \quad (3.13)$$

### 3.3 Numerical Computation

The radial velocities at the (j+1)th station are computed from equation (3.13). The  $U_0$  and  $V$  appearing in the coefficients of equations (3.10), (3.11) and (3.13) are considered to be known values at the node (j+1,k). In the computation, the  $U_{0,j,k}$  and  $V_{j,k}$  are first used in the coefficients to obtain  $U_{0,j+1,k}$  and  $V_{j+1,k}$ . The iterative process of replacing the previous values of  $U_{0,j+1,k}$ ,  $V_{j+1,k}$  by present values is continued until satisfactory values for  $U_{0,j+1,k}$  and  $V_{j+1,k}$  are obtained which satisfy the fundamental equations exactly. Although Pai and Hsieh [10,11] used the same method to solve the fundamental equations the computer program used by them is found to have an error (Appendix D).

Although the boundary of the free jet is at infinity, due to the limitation on the numbers a computer could handle, the solution is started with 1350 grid points at the nozzle exit in the transverse direction. The computation is started with the mesh sizes of 0.001 in the radial direction and  $2.5 \times 10^{-4}$  in the axial direction. As the computation proceeds downstream the number of grid points in the radial direction and the mesh sizes are increased in such a way that the convergence of the solution is still achieved. Increasing the number of grid points more than the above mentioned values does not change the solution significantly.

It is worth mentioning here that although the implicit finite difference technique is free of stability problems the solution would

converge only if the number of iterations on  $U_0$  and  $V$  are infinite for any arbitrarily large or small mesh size. Since the number of iterations on  $U_0$  and  $V$  were fixed at specific values it was necessary to determine the proper mesh size. The starting value of the axial step size is determined from the stability criterion for an explicit difference method which is  $\frac{\Delta X}{(\Delta Y)^2} < \frac{1}{2}$  where the initial value for the radial step size is chosen as .001. With these step sizes the solutions at an axial distance 0.001 downstream of the nozzle exit are obtained. The solutions at the same location are again obtained with the axial step size halved. Both solutions are compared. If the axial velocities are correct up to four significant figures and the local error in the radial velocities are less than 5% then it is said that the convergence has been achieved. If the solution does not converge the step size is repeatedly halved until the solution has converged. When this occurs, the computation is continued with the admissible large step size in the X direction. As the computation proceeds downstream the axial and the radial step sizes are gradually increased in accordance with the convergence criteria described above. The numerical procedure described above is coded into a Fortran program (Appendix A). This program is a modified version of that used by Pai and Hsieh [10,11].

### 3.4 Analysis of the Finite Difference Solution

As previously stated the main aim of this work is to model the velocity profile in the developing region of the jet. A combination of a parabolic and a Schlichting profile is suggested in this

region as shown in Figure 1. The region close to the axis of the jet is considered to be of parabolic form with reduced centre line velocity based on the experimental data [12]. Far downstream, the Schlichting velocity profile represents the velocity distribution. Therefore it is reasonable to approximate the free shear layer which surrounds the parabolic core by a Schlichting jet with its axis shifted.

To verify whether there is a parabolic region and, if there is such a region, to determine its radial width a subroutine called GUNAM is written. This subroutine GUNAM generates a parabolic velocity profile and compares the magnitude of these velocities with the axial velocities obtained from the finite difference solution. When the difference is larger than the predetermined tolerance, the subroutine records the radial distance where this occurs and takes this as the width of the parabolic core. The other subroutines HALU and MYLV that appear in the main program determine the value of  $R_{m/2}$  and the values of  $U/U_0$  with  $R/R_{m/2}$  respectively at the required axial locations. The flow charts and the listing of the main program and the subroutines are given in the Appendix A.

#### 3.4.1 Schlichting Velocity Profile in the Free Shear Layer

The equation of the Schlichting velocity profile in free shear layer in the developing region can be written in the non dimensional form as:

$$U_0 = \frac{2(\gamma/Re_c)^2}{(X_c + X_{cv})} \left[ 1 - \left( \frac{\gamma}{2Re_c} \frac{(R-A)}{(X_c + X_{cv})} \right)^2 \right]^{-2} \quad (3.14)$$

The unknown coefficients in equation (3.14) are  $\gamma/Re_c$  and A.

The data points  $U_0$  and R obtained from the finite difference solution at particular axial locations were used in the program NLIN, available in the University of Windsor Computer Centre Statistical Analysis Program Library [3], to determine  $\frac{\gamma}{Re_c}$ ,  $X_{cv}$  and A. A modified Gauss-Newton method is employed in the NLIN program to estimate the unknown coefficients. The program requires the description of the model, its partial derivatives with respect to the coefficients A,  $(X_{CV}+X_C)$  and  $\frac{\gamma}{Re_c}$ , and the anticipated ranges of values of these coefficients.

### 3.5 Simplified Derivation of the Maximum Velocity Decay

The momentum equation for the axisymmetric jet along the axis and with boundary layer approximations can be written as,

$$U_m \frac{d U_m}{d X_c} = \left( \frac{\partial^2 U_0}{\partial R^2} + \frac{1}{R} \frac{\partial U_0}{\partial R} \right)_{R=0} \quad (3.15)$$

Using L Hopital's rule it can be shown that:

$$\frac{\frac{\partial U_0}{\partial R}}{R} \Big|_{R \rightarrow 0} = \frac{\frac{\partial^2 U_0}{\partial R^2}}{1} \Big|_{R \rightarrow 0} \quad (3.16)$$

Therefore the momentum equation can be rewritten as:

$$U_m \frac{dU_m}{dX_c} = 2 \left( \frac{\partial^2 U_0}{\partial R^2} \right)_{R=0} \quad (3.17)$$

For the case when the velocity profile is parabolic at the tube exit the centre line velocity is a local mathematical maximum,  $\frac{\partial^2 U_0}{\partial R^2} < 0$  at  $R = 0$ . As a result, equation (3.17) gives



$U_m \left( \frac{dU_m}{dx_c} \right) < 0$ . Therefore,  $\frac{dU_m}{dx_c} < 0$  because  $U_m > 0$ . This shows that the centre line velocity begins to decrease immediately at the tube exit.

### 3.5.1 Variation of Maximum Velocity with Axial Distance

An approximate solution for the axial variation of centre line velocity will now be considered. As the fluid exits from the tube it comes into contact with the surrounding stationary fluid. The edges of the velocity profile are changed from the parabolic shape that exists at the tube exit. The central portion, however, remains approximately parabolic with the centre line maximum velocity reduced from the value at the exit. This aspect of the jet flow has been noticed from the results of finite difference solution described in Section 3.4 and from the measurements of Rankin [12]. As the fluid moves downstream, the region where the velocity profile is parabolic becomes smaller. At a particular distance from the nozzle exit ( $x - x_0$ ) the velocity profile reduces to that of Schlichting as shown in Figure 1.

In the developing region the parabolic portion of the velocity profile in nondimensional form is given by,

$$U_0 = U_m (1 - R^2) \quad (3.18)$$

where  $U_m$  is a function of  $x_c$ .

The first and the second derivatives of  $U_0$  with respect to  $R$  can be obtained from equation (3.18). They are:

$$\frac{\partial U_0}{\partial R} = -2 U_m R \quad (3.19)$$

$$\frac{\partial^2 U_0}{\partial R^2} = -2 U_m \quad (3.20)$$

Substituting for  $\frac{\partial^2 U_0}{\partial R^2}$  in equation (3.53) gives,

$$\frac{dU_m}{dX_c} = -4 \quad (3.21)$$

Integrating the equation (3.21) gives,

$$U_m = -4 X_c + C \quad (3.22)$$

where C is an arbitrary constant.

At the nozzle exit;  $X_c = 0$ ,  $U_m = 1$ . Substituting this condition in the equation (3.22) yields,

$$C = 1 \quad (3.23)$$

Therefore,

$$U_m = 1 - 4 X_c \quad (3.24)$$

It should be recalled that equation (3.24) applies in the developing region ( $0 < X_c < X_{cl}$ ). In the fully developed region the velocity profile is given by Schlichting's solution.

$$U_o = \frac{2(\gamma/Re_c)^2}{(X_c + X_{cv})} \left[ 1 + \left( \frac{1}{2} \frac{\gamma}{Re_c} \frac{R}{(X_c + X_{cv})} \right)^2 \right]^{-2} \quad (3.25)$$

where  $X_{cv}$  is the nondimensional distance to the virtual origin, upstream of the jet exit, as shown in Figure 2. When  $R = 0$ , equation (3.25) gives the centre line velocity distribution along the axis of the jet in the fully developed region ( $X_{cl} < X_c < \infty$ ),

$$U_m = \frac{2(\gamma/Re_c)^2}{(X_c + X_{cv})} \quad (3.26)$$

Since one of the assumptions is that momentum is conserved in a submerged free jet and the initial velocity profile is parabolic, the constant  $\gamma/Re_c$  can be determined.

The momentum of the jet [1] is,

$$J = 2\pi \rho \int_0^{\infty} u^2 r dr = \frac{16}{3} \pi \rho \gamma^2 v^2 \quad (3.27)$$

The momentum of the jet at the exit of the nozzle is

$$J = \int_0^a 2\pi \rho u^2 r dr = \frac{1}{3} \pi \rho u_{mo}^2 a^2 \quad (3.28)$$

By setting equations (3.27) and (3.28) equal to one another it can be shown that,

$$\frac{\gamma}{Re_c} = \frac{1}{4} \quad (3.29)$$

Therefore equation (3.26) reduces to

$$U_m = \frac{1/8}{(X_c + X_{cv})} \quad (3.30)$$

### 3.5.2 Matching of Maximum Velocity Variations

In this section the  $U_m$  variations in the developing and fully developed regions, Equations (3.24) and (3.30), are matched to obtain the length of the developing region ( $X_{cl}$ ) and the distance of the virtual origin ( $X_{cv}$ ). The conditions of matching are as follows;

At  $X_c = X_{cl}$ ,

- (i)  $U_m$  given by equations (3.24) and (3.30) are equated.
- (ii)  $\frac{dU_m}{dX_c}$  obtained from equations (3.24) and (3.30) are equated.

The following two equations are obtained from the matching:

$$1 - 4X_{cl} = \frac{1/8}{X_{cl} + X_{cv}} \quad (3.31)$$

$$-4 = \frac{-1/8}{(X_{cl} + X_{cv})^2} \quad (3.32)$$

Equations (3.31) and (3.32) are solved to get the values of  $X_{cl}$  and  $X_{cv}$ . We find

$$X_{cv} = 2\left(\frac{1}{8 \times 4}\right)^{\frac{1}{2}} - \frac{1}{4} = 0.1036 \quad (3.33)$$

and

$$x_{cl} = \frac{1 - \sqrt{4 \times 1/8}}{4} = 0.0732 \quad (3.34)$$

The values of the root in equations (3.33) and (3.34) are taken in a consistent way to yield a positive value for  $x_{cv}$ . In other words, the virtual origin for the Schlichting's solution is located inside the jet nozzle.

CHAPTER IV  
RESULTS AND DISCUSSION

4.1 Finite Difference Solution

The finite difference solution of the boundary layer equations (3.3) and (3.4) are presented in Table I. These results are discussed in detail in the following sections.

4.1.1 Centre Line Velocity Variation

The axial velocity profiles are computed from the momentum equation. The variation of non-dimensional centre line velocity with the non-dimensional axial distance is plotted in Figures 3 and 4. The above results are also presented in tabular form in Table I. In Figure 3 the variation is compared with the experimental results. The experimental results of Rankin [12] are considered to be more reliable than those of other investigators since a Laser Doppler Anemometer is used to measure the velocities. This device is preferred because it doesn't interfere with the flow. The present numerical results agree well with Rankin's [12] experimental results. Since Rankin has compared his results extensively with those of others [1, 15, 16] they are not presented here.

Figure 4 shows the comparison of the present centre line velocity variation with the other analytical results. For  $X_c$  greater than 0.028, Pai and Hsieh's [10, 11] numerical solution is in good agreement with the present results. The disagreement when  $X_c$  is less than 0.028 could possibly be due to larger step sizes used by them in that range. It is also not clear from their paper whether they did achieve convergence of their solution in the near exit

region of the jet. The correlation of Dmitriev and Kulesovā is in excellent agreement, however, the variation suggested by them has a discontinuity at the boundary of developed and developing region. This discontinuity is a result of the method used to determine the development length of the jet.

Rankin's theoretical model shows good agreement with the present solution when  $X_c$  is less than 0.04. The agreement with the increasingly worse as the value of  $X_c$  becomes larger. The increasing divergence is due to the fact that his velocity profile model does not converge towards a Schlichting profile.

#### 4.1.2 Parabolic Core of the Jet

The extent of the parabolic core has been determined by a subprogram called "GUNAM". In the parabolic core, the velocity profile remains almost parabolic but with reduced centre-line velocity. The variation of the width of the parabolic region with the non-dimensional axial distance is plotted in Figure 5 for the tolerance values of 0.001 and 0.005. From Figure 5 it is apparent that the width of the parabolic core depends upon the preset tolerance value of the generated parabolic profile and the velocity field obtained from the finite difference technique. However, the uncertainty analysis on the parabolic velocity (Appendix B) indicates that the uncertainty of the axial velocity normalized with the local centre line velocity is  $\pm 0.001 R$ . This shows that even in the case of an exact parabolic profile there is an uncertainty on  $U_0$ . For this reason the smallest step size in the radial direction used in the finite

difference calculations has been chosen as the tolerance value for the determination of  $R_p$ .

Figure 5 shows a steep drop in the width of the parabolic core in the very near region of the nozzle exit. The change in  $R_p$  is very small when  $X_c$  is larger than 0.06 due to the fact that the parabolic and Schlichting profiles coincide in this region. Since the curve  $R_p$  vs  $X_c$  does not intersect the x axis anywhere in between 0 and 0.1 it seems that the flow has not yet developed. An approximate method of locating the end of parabolic region in the axial direction is presented in Section 3.5.2.

#### 4.1.3, Jet Half-Radius

The variation of  $R_{m/2}$  with the axial distance, given in Table I, provides an excellent means of representing the spread of the jet. This variation is plotted in Figure 6 along with the results of Rankin [12] and Pai and Hsieh [10, 11]. For the range of  $X_c$  from 0. to 0.06 Rankin's experimental results are in good agreement with the present numerical solution, however, at larger axial distances his data indicate a wider jet. The theoretical results of Rankin show a broader jet by about 5.6%. Pai and Hsieh approximated their numerical solution, for the range of  $X_c$  from 0.1 to 2.0, by a straight line given by

$$R_{m/2} = 5.2 (X_c + 0.1) \quad (5.3)$$

A nonlinear variation of the jet width is indicated when  $X_c$  is less than 0.1. The present numerical solution shows good agreement with



the equation (5.3) when  $X_c$  is greater than 0.06.

#### 4.1.4 Axial Velocity Profiles

The axial velocity distributions are presented in Table I. The axial velocity distributions are compared with the Schlichting velocity profile in Figure 7. The comparison is made by plotting  $\frac{U_o}{U_m}$  at constant  $\frac{R}{Rm/2}$  against  $X_c$ . For the similar solution  $\frac{U_o}{U_m}$  is constant at constant  $\frac{R}{Rm/2}$  but in the developing region the numerical solution shows that  $\frac{U_o}{U_m}$  depends both on  $\frac{R}{Rm/2}$  and  $X_c$ . However, as  $X_c$  increases, the numerical solution approaches Schlichting's solution.

#### 4.2 Velocity Model in the Developing Region

In Section 4.1 it has been shown that in the developing region the velocity field of the cylindrical portion of the jet which surrounds the axis can be represented by a parabolic velocity profile. The finite difference solution outside of this parabolic core is used along with a nonlinear curve fitting technique to determine the parameter of the modified Schlichting velocity profile that best fits the numerical solution in this region. The non-dimensional axial locations and their corresponding Schlichting parameters namely  $X_{cv}$ ,  $\frac{Y}{Re_c}$  and A are presented in Table 3 and in Figure 8, 9 and 10. These parameters are determined by using a standard library program called "NLIN". In order to maintain a reasonable computer time, approximately 140 equally spaced points are used. The Schlichting parameters are constant in the fully developed region of the jet and they are independent of  $X_c$ . The above figures indicate that the flow is still developing at an axial distance as large as 0.1 since they have not reached constant values. Axial velocity distribution in the free shear layer are generated

by using the Schlichting parameters obtained above in equation (3.14). Figures 11 to 19 show the finite difference solutions plotted against their corresponding parabolic and Schlichting velocity models at different axial locations. In these plots the origin and the point farthest away from the origin corresponds to the edge and the axis of the jet respectively. As anticipated in the region near the axis of the jet the parabolic velocity model is in excellent agreement with the numerical solution. The modified Schlichting model in the free shear layer exhibits an acceptable agreement with the finite difference solution. However, in the region near the edge of the jet the finite difference solution diverges slightly from the modified Schlichting model. This could possibly be due to the restriction placed on the width of the jet.

#### 4.3 Simplified Derivation of the Variation of Axial Velocity

Equation (3.17) may be used to predict the manner in which the centre line velocity would change knowing initial velocity profile of the jet at the tube exit. Consider the case when the initial velocity profile of the jet at the exit of the tube is uniform. In this case, points in the jet are said to be in the developing region as long as a potential core exists. In the potential core the velocity profile is uniform and  $\partial^2 u / \partial r^2 = \partial u / \partial r = 0$ . Therefore, clearly from equation (3.17) we see that  $U_m$  remains constant in the developing region. Consider the intermediate case where the tube length is inadequate to produce a fully developed laminar pipe flow. In this case, the edges of the profile are approximately parabolic and the central portion is uniform. Using the same argument as in the previous case, it can be

shown that the centre line velocity remains constant in the developing region.

Equation (3.24) indicates that the nondimensional maximum velocity decays linearly in the developing region of a laminar jet that has a parabolic velocity profile at the nozzle exit. Dmitriev and Kulesova [7] have obtained exactly the same relationship, by fitting a curve to a finite difference solution of the boundary layer equations. From Figure 4 it can be seen that equation (3.24) is also an excellent fit for the present finite difference solution. The present derivation of this equation is certainly preferable in view of the simple, basic assumptions that have been made and the implication that they have on the jet structure; namely, the existence of a parabolic core region similar to a potential core in the uniform exit velocity case. The parabolic portion of the velocity profile experiences a uniform rate of decrease in the maximum velocity but not a change in shape. This region is relatively unaffected by the entrainment compared to the outer edges of the jet. In view of the fact that the radial velocity component approaches zero, the use of the boundary layer assumptions for a differential element along the jet centre line is certainly justified.

The present method of matching the solution in the developing and fully developed regions is unique in that it occurs at the end of the developing region and includes a match of axial velocity gradient as well as the velocity. This results in a determination of both  $X_{cv}$  and  $X_{cl}$ . Traditionally, [2, 4, 5] jet matching has been accomplished at the tube exit and involves matching one of a number of possible

quantities of the exit flow condition to that of Schlichting's similarity profile. This results in a determination of  $X_{cv}$  only, but not  $X_{cl}$ . Flow quantities matched in the literature include kinetic energy, centre line velocity, volume flow rate and streamlines at the edge of the tube exit. The resulting  $X_{cv}$  values, along with references are included in Table 2 for comparison with the present case. Also included is the result of du Plessis et al. [8] which was obtained by comparing the similarity profile with a numerical finite difference solution to estimate  $X_{cv}$  and  $X_{cl}$ . Tsang [16] obtained his values by comparing with a slightly different numerical method. The values of  $X_{cv}$  and  $X_{cl}$  given by Chang [6] were determined from experimental velocity profile data. The dependence of  $X_{cl}$  upon  $Re_c$  is unique among the results and yields a value of  $x_q/a = 20$ . The lack of  $Re_c$  dependence of  $x_q/a$  is likely due to the narrow range of  $Re_c$  values used in his tests ( $Re_c = 430$  and  $600$ ).

The results of Dmitriev and Kulesova [7] were obtained by approximately matching the maximum velocity in the development region, equation (3.17), to that in the fully developed region assuming a value of  $X_{cv}$  equal to that for kinetic energy matching. The two curves do not join and hence a discontinuity exists in their method. The present values are in good agreement with Dmitriev and Kulesova's [7], however, yield results without any discontinuity. By allowing the values of  $X_{cv}$  and  $X_{cl}$  to be determined simultaneously less restriction was placed on the solution. The present values of  $X_{cv}$  and  $X_{cl}$  are in slightly better agreement with the values of du Plessis et al. [8].

A better comparison can be made by constructing a graph of  $U_m$  versus  $X_c$  as given in Figures 20 and 21.

The experimental and analytical results of Rankin [12] and the numerical finite difference solution of Pai and Hsieh [10, 11] further substantiate the accuracy of the present approximation.

CHAPTER V  
CONCLUSIONS

5.1 Finite Difference Solution

- (1) The finite difference solution of the boundary layer equations for the case of an axisymmetric jet issuing from a wall with parabolic exit velocity profile into an infinite expanse of fluid is presented in a useful tabular manner.
- (2) Based on the finite difference solution, a velocity distribution model for the developing region of the jet formed by the combination of parabolic and Schlichting velocity profiles is presented.

5.2 Simplified Derivation of Maximum Velocity Decay

- (1) A maximum velocity decay relationship, based on the momentum equation applied along the jet centre line and the use of the boundary layer assumptions, has been developed which:
  - (a) proves that the maximum velocity in a laminar jet remains constant only if a potential core exists, and decreases in every other case.
  - (b) predicts a linear variation of the maximum velocity in the development region if we assume that a central parabolic core exists.
- (2) A scheme for matching the maximum velocity and its gradient in the axial direction at the end of the development

region is presented and shown to yield an estimate of

$\rho$   $X_{cl}$  as well as  $X_{cv}$ .

- (3) The resulting combined model for the centre line velocity is in good agreement with the experimental and more exact methods of analysis.

REFERENCES

- [1] Abramovich, S. and Solan, A., "The Initial Development of a Submerged Laminar Round Jet", *Journal of Fluid Mechanics*, Vol. 53, part 4, 1973, pp 791-801.
- [2] Andrade, E.N. and Tsien, L.C., "The Velocity Distribution in a Liquid into Liquid Jet", *Proceedings of the Physical Society, London*, vol. 49, Part 4, 1937, pp 381-391.
- [3] Barr, J., Goodnight, H., Sall, P. and Helvig, T., "A Users Guide to SAS.76", SAS Institute Inc. 1976, pp 193-199.
- [4] Bell, A.C., "An Analytical and Experimental Investigation of the Turbulence Amplifier", S.C.D. thesis, Mechanical Engineering Department, Massachusetts Institute of Technology, 1969.
- [5] Bell, A.C., "The Turbulence Amplifier, Static and Dynamic Characteristics", *Fluidics Quarterly*, vol. 7, Number 4, 1975, pp 1-52.
- [6] Chang, H., "An Analytical and Experimental Investigation of a Large-Scale Model of a Turbulence Amplifier", M.Sc. thesis, State University of New York at Buffalo, 1972.
- [7] Dmitriev, V.N. and Kulesova, N.A., "The Calculation of a Laminar Jet in the Surroundings of the Supply Nozzle", *Proceedings of the "Jablonna" Fluidics Conference*, Budapest, Hungary, Nov. 1974, pp 83-91.
- [8] du Plessis, M.P., Wang, R.L. and Tsang, S., "Development of a Submerged Round Laminar Jet from an Initially Parabolic Profile", *ASME Journal of Dynamic Systems, Measurement and Control*, Vol. 94, 1973, pp 148-154.
- [9] Landau, L.D., "A New Exact Solution of the Navier-Stokes Equations", *Collected papers of L.D. Landau*, 2nd ed., D. Ter Harr ed., Gordon and Breach, Science Publishers, 1967, pp 383-386.
- [10] Pai, S.I. and Hsieh, T., "Numerical Solution of Laminar Jet Mixing with and without Free Stream", Technical Note BN-627, United States Army Material Command, Harry Diamond Laboratories, Nov. 1969.
- [11] Pai, S.I. and Hsieh, T., "Numerical Solution of Laminar Jet Mixing with and without Free Stream", *Applied Scientific Research*, Vol. 27, 1972, pp 33-62.



- [12] Rankin, G.W., "Developing Region of Laminar Jets", Ph.D. Dissertation, University of Windsor, Ontario, Canada, 1980.
- [13] Rumer, Y.B., "Problem of Submerged Jet", Prikladnaja Matematika i Mekani, Vol. 15, 1952, pp 255-256.
- [14] Schlichting, H., "Boundary Layer Theory", Sixth Edition, McGraw-Hill Book Company (1968).
- [15] Symons, E.P. and Labus, T.L., "Experimental Investigation of an Axisymmetric Fully Developed Laminar Free Jet", NASA TN D-6304, 1971.
- [16] Tsang, S., "A Study of Axisymmetric Submerged Jets Relevant to Turbulence Amplifier Design", Masters thesis, Dept. of Mechanical Engineering, Sir George Williams University, Montreal, Canada, August 1971.

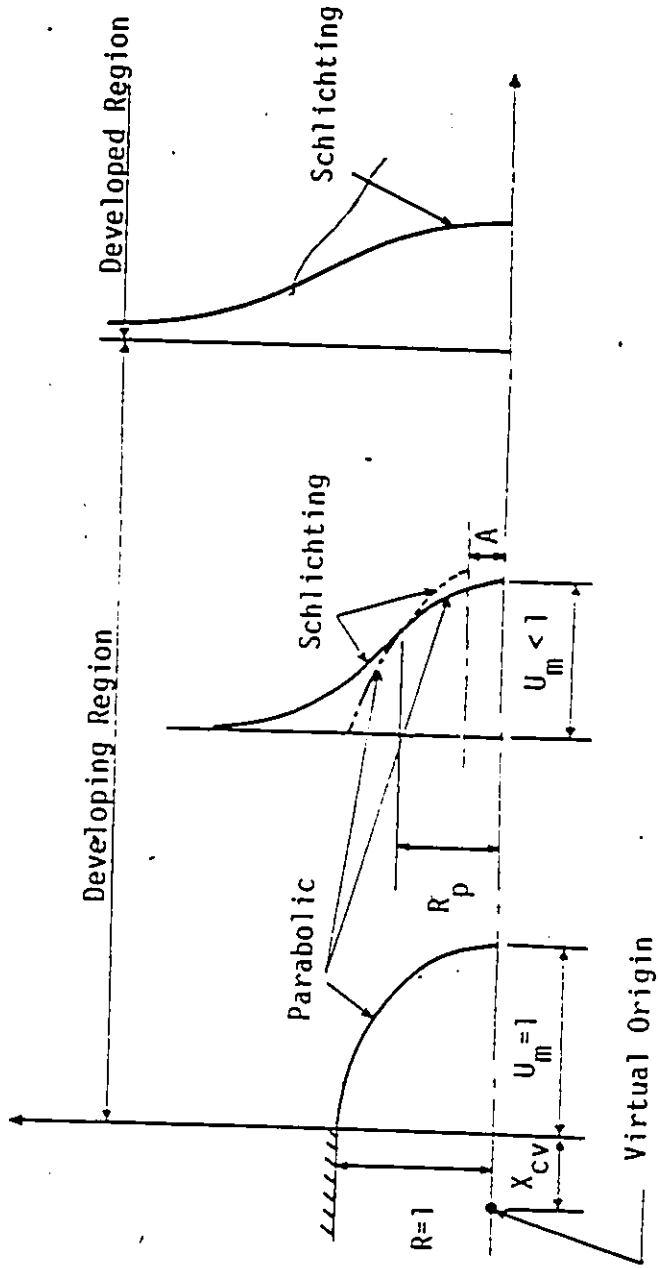


Figure 1 Velocity Profile Model

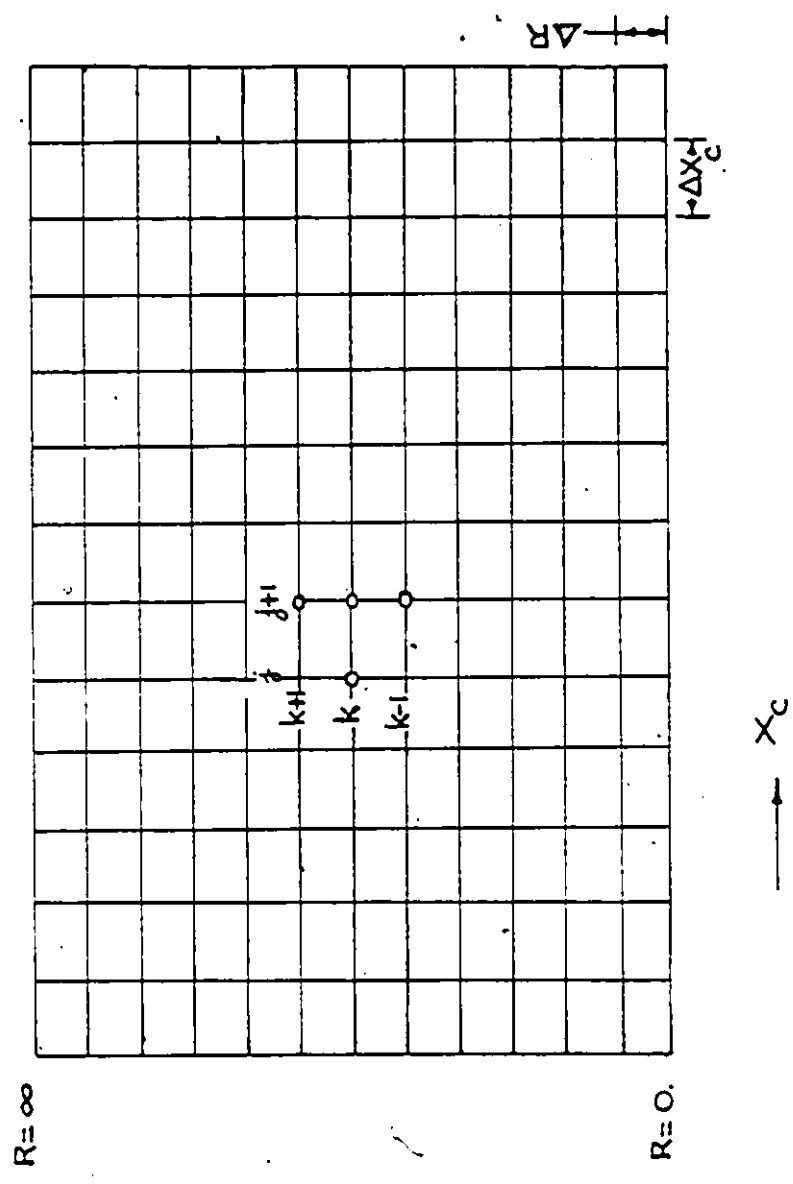


Figure 2 Finite Difference Grid

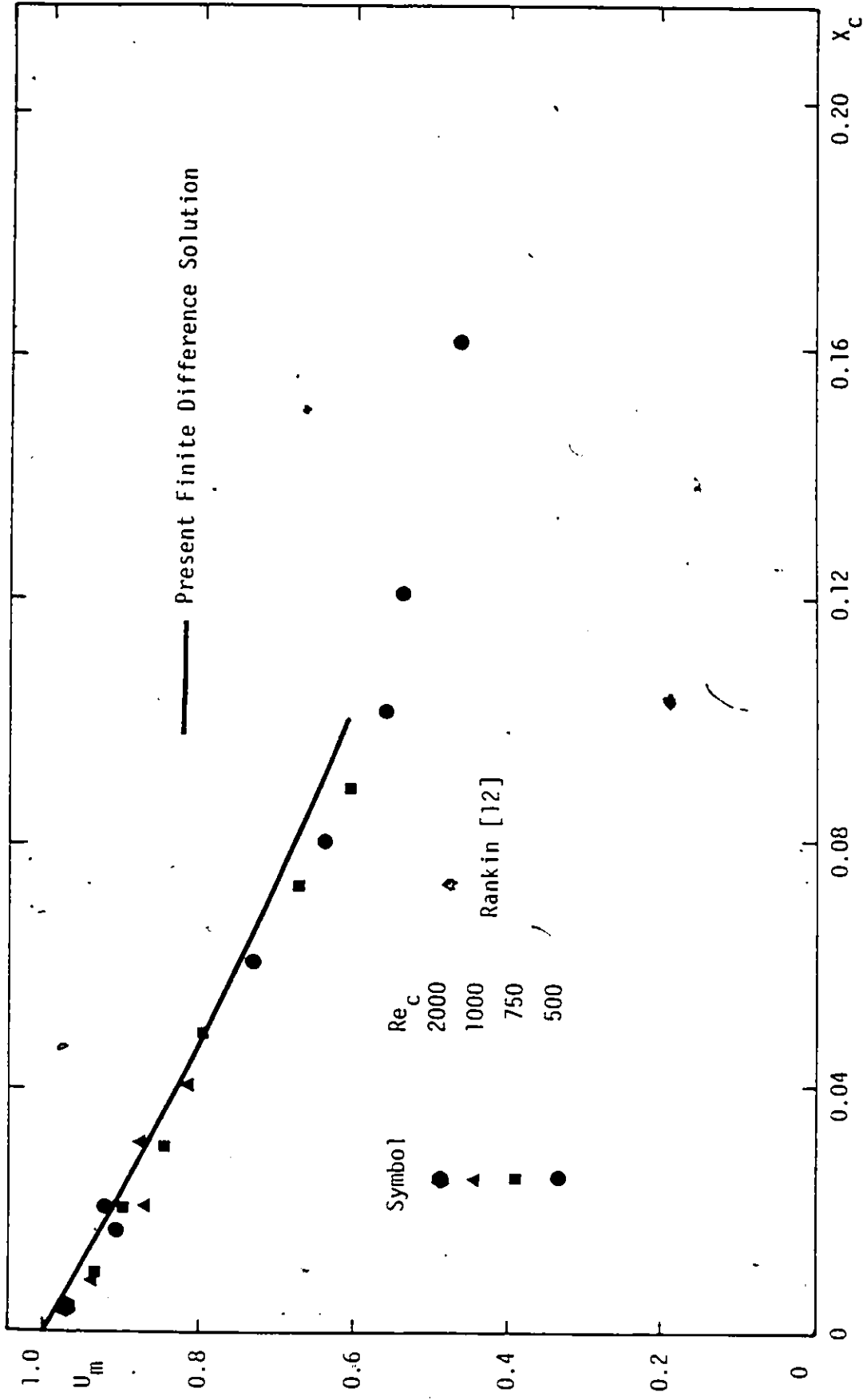


Figure 3 Experimental Centre Line Velocity Decay.

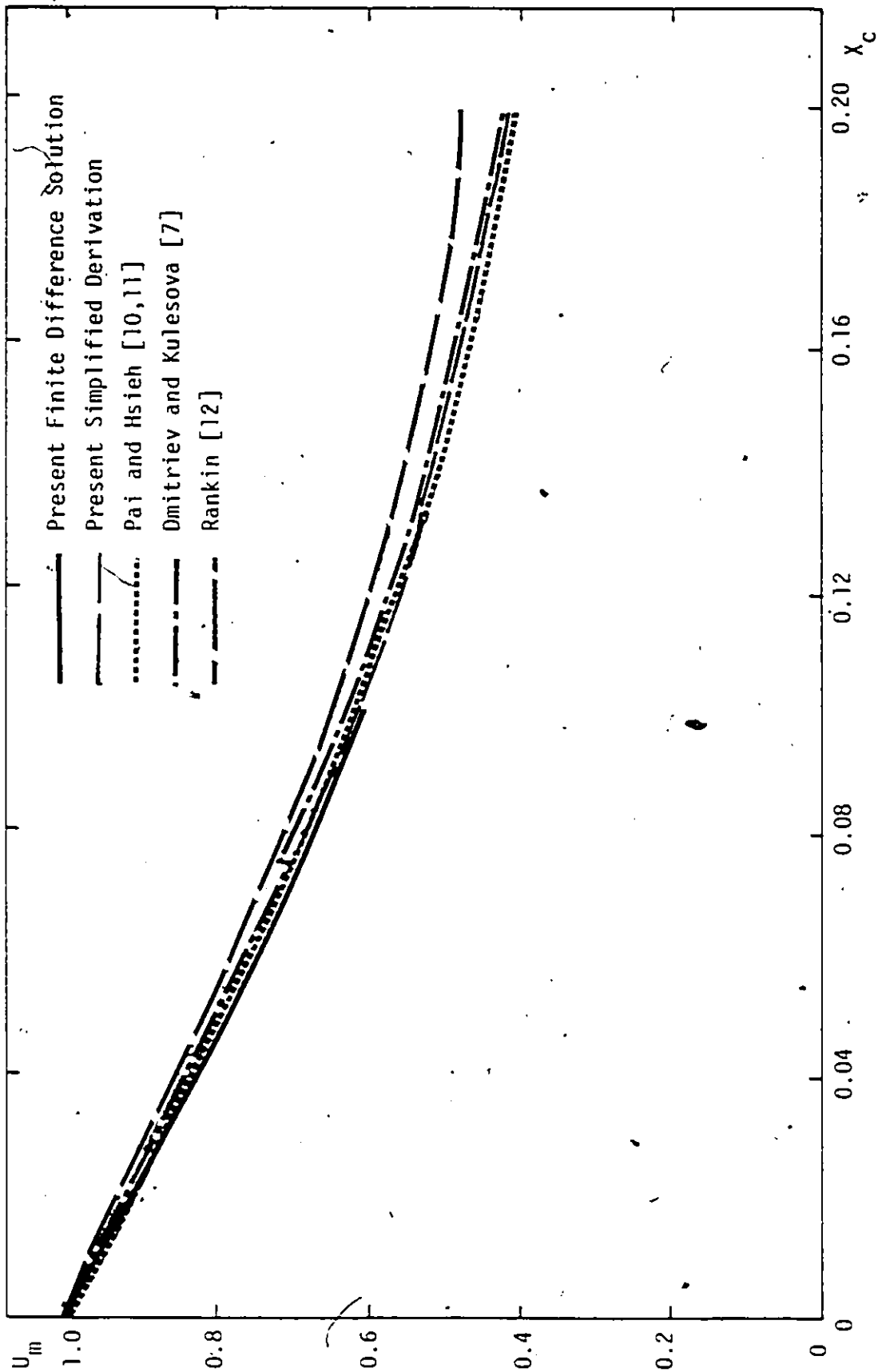


Figure 4 Analytical Centre Line Velocity Decay.

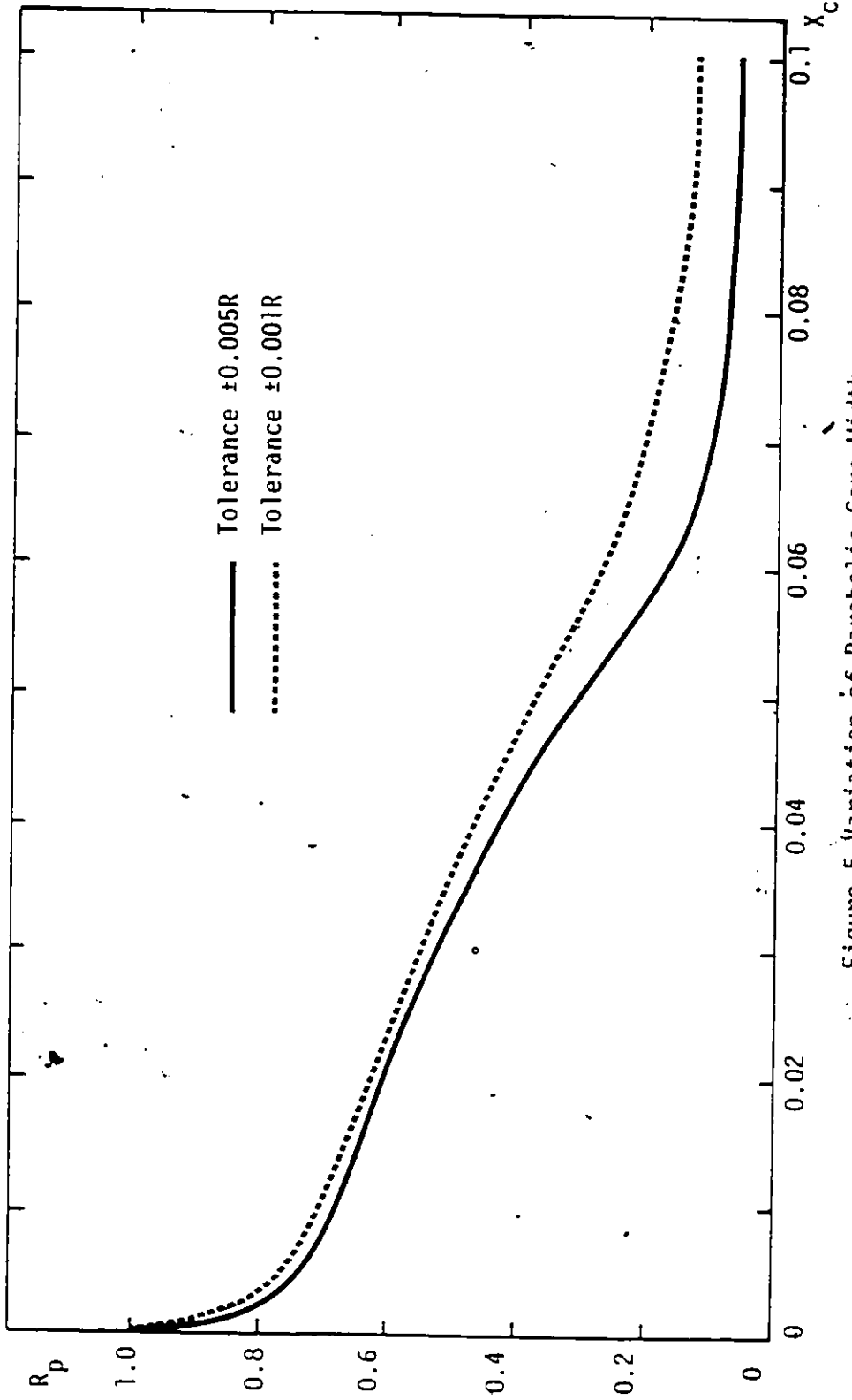


Figure 5 Variation of Parabolic Core Width.

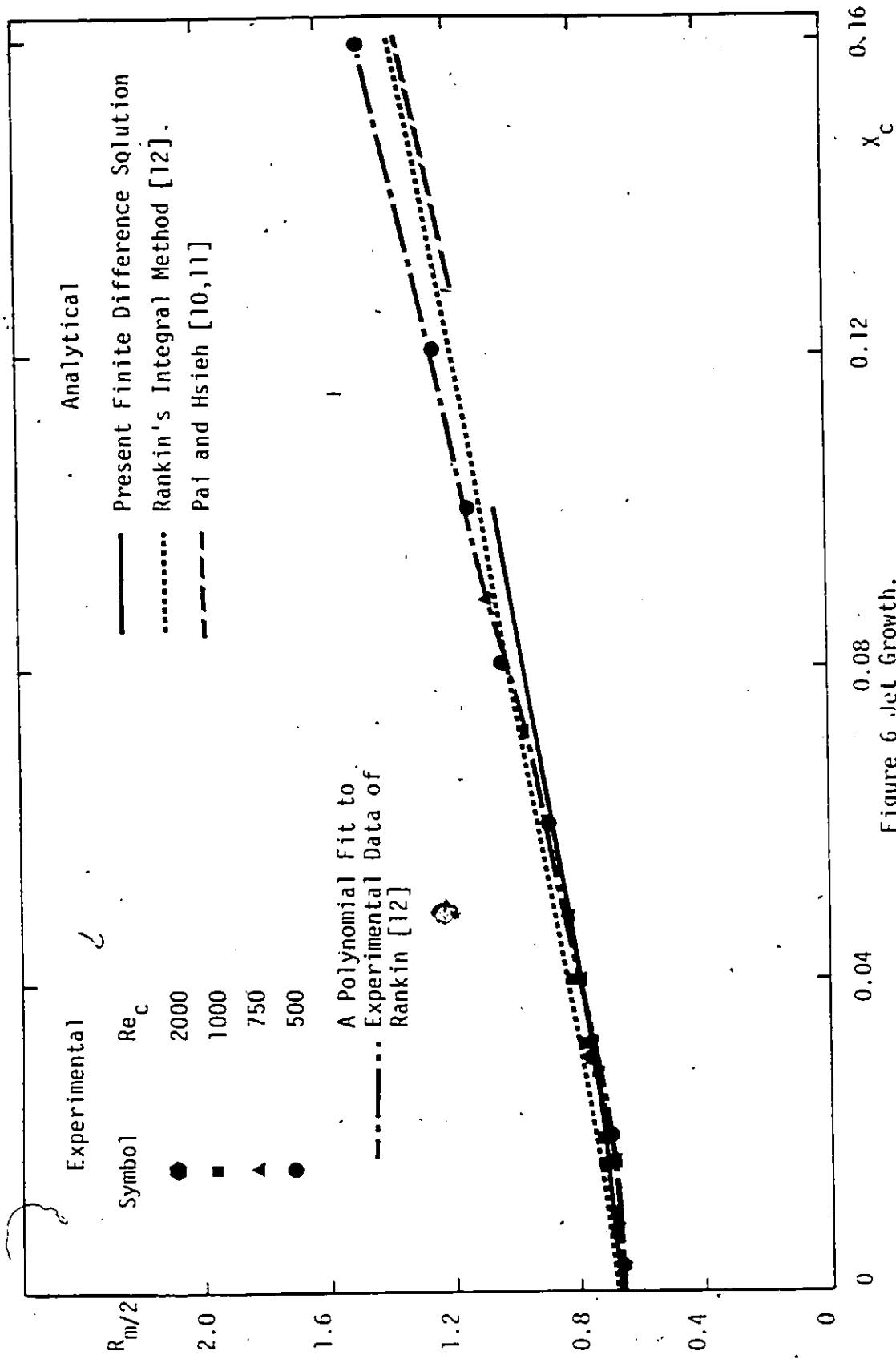


Figure 6 Jet Growth.

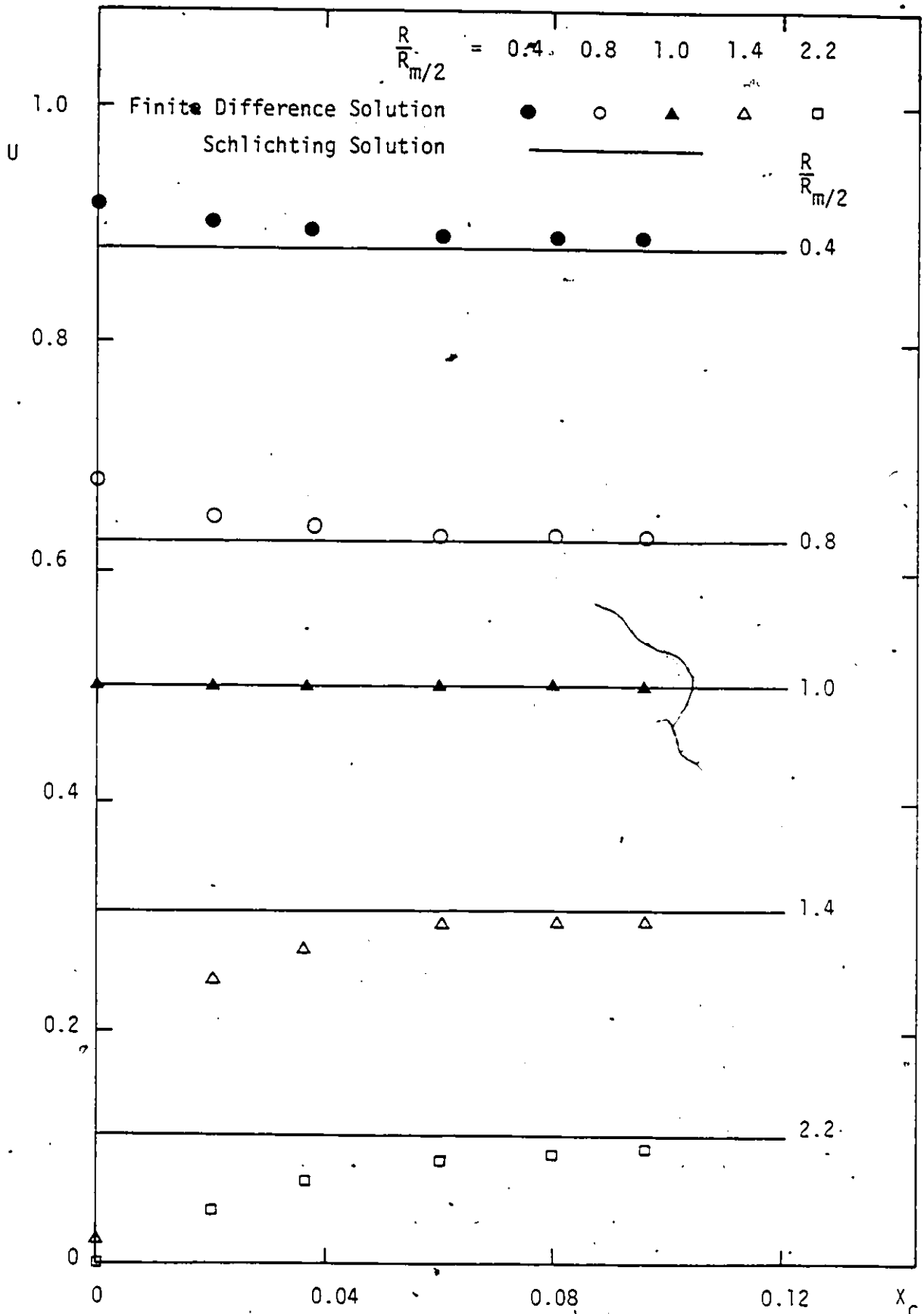


Figure 7 Velocity Variation at Different Radial Locations.



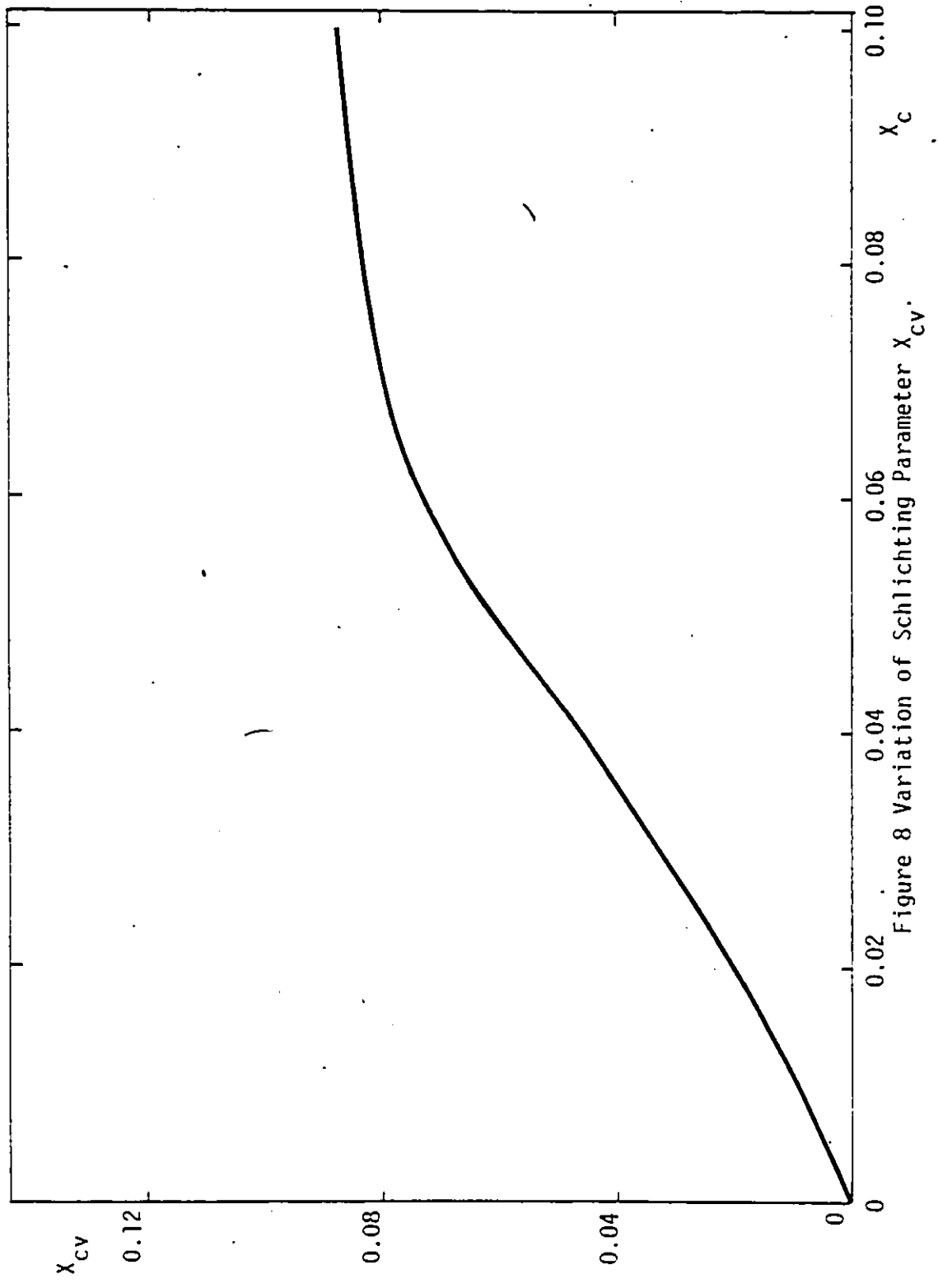


Figure 8 Variation of Schlitching Parameter  $X_{cv}$ .

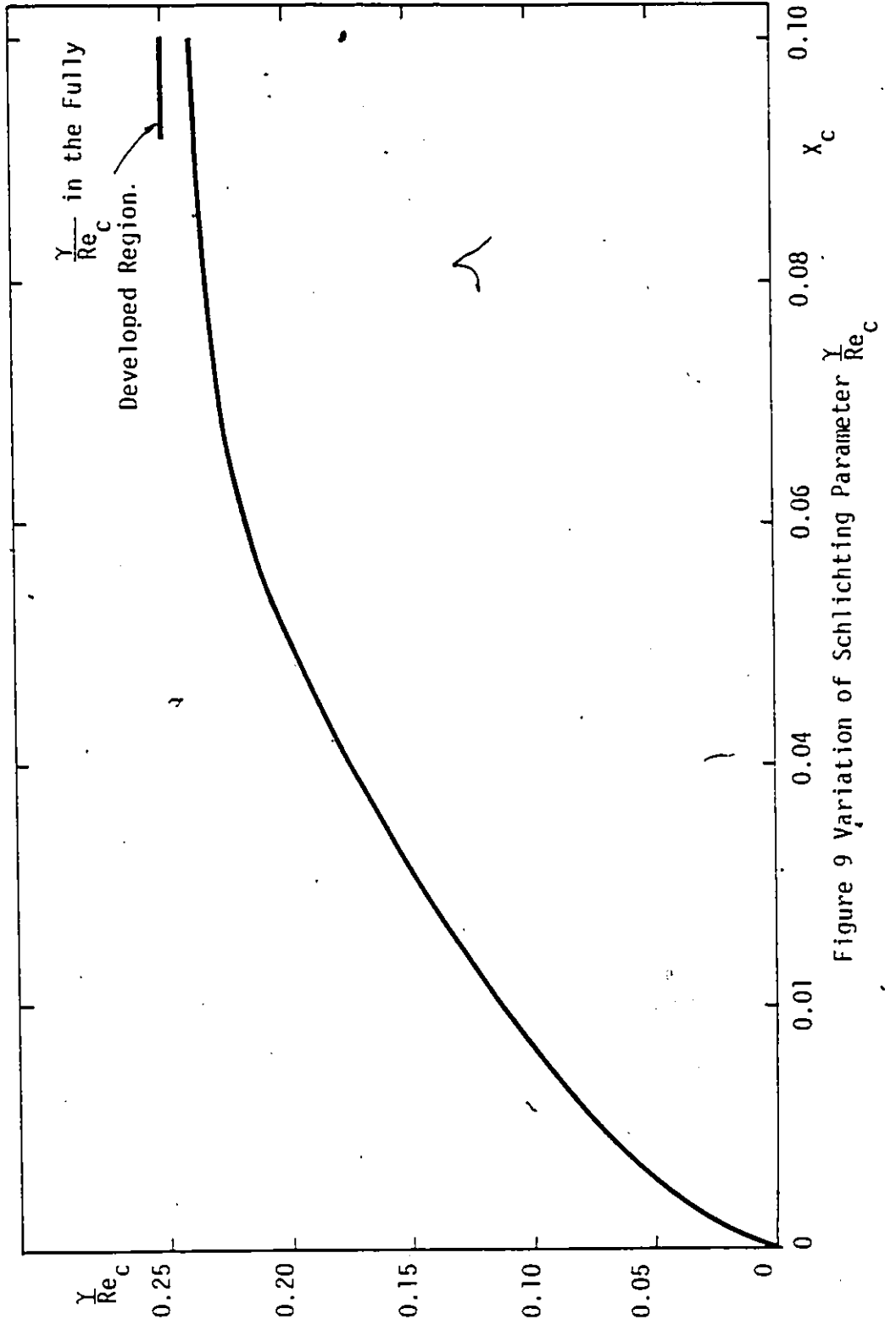


Figure 9 Variation of Schlichting Parameter  $\frac{Y}{Re_c}$

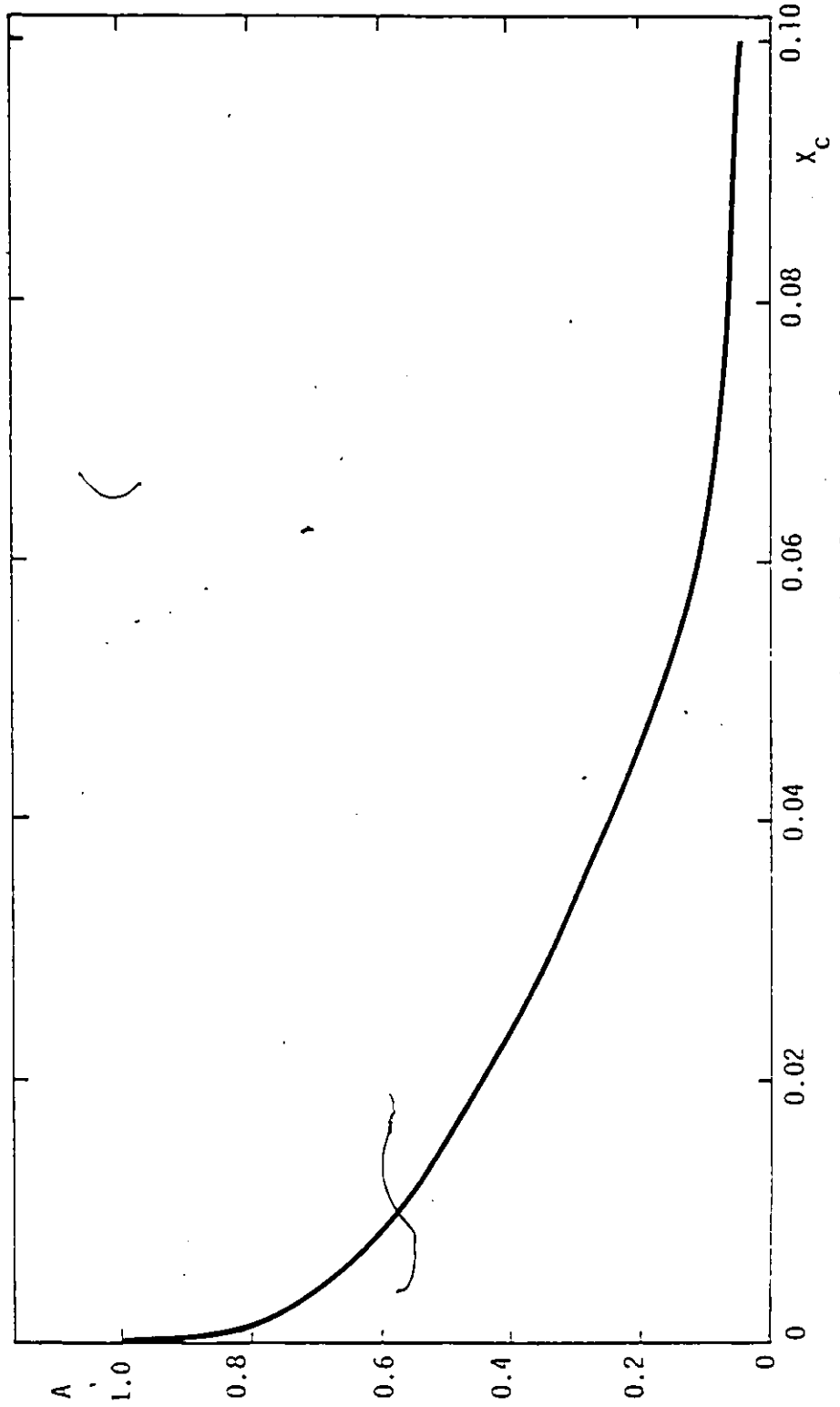


Figure 10 Variation of Schlichting Parameter A.

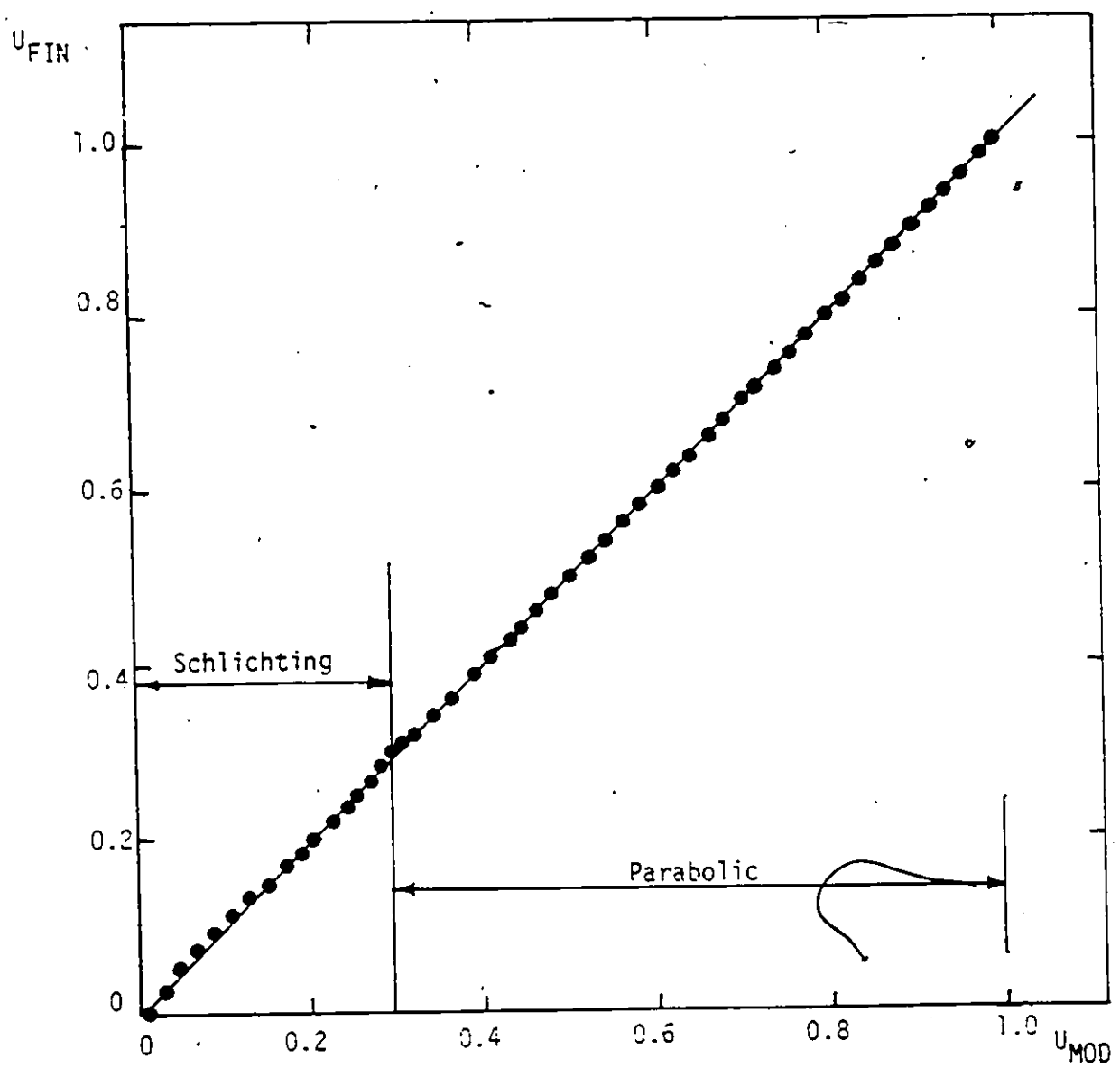


Figure 11 Comparison of Velocity Profile Model and Finite Difference Solution ( $X_c=0.001$ )

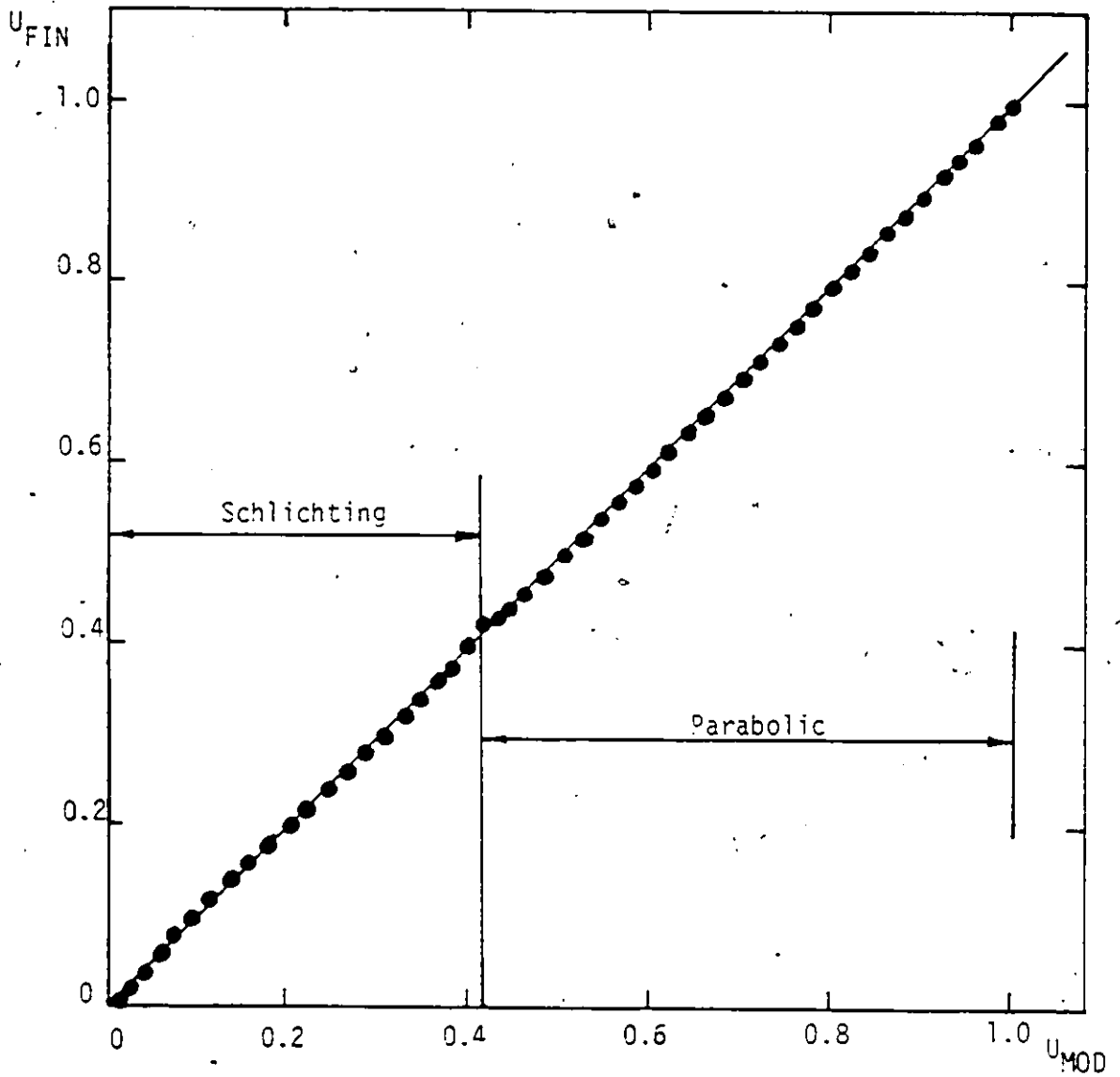


Figure 12 Comparison of Velocity Profile Model and Finite Difference Solution ( $X_c=0.004$ )

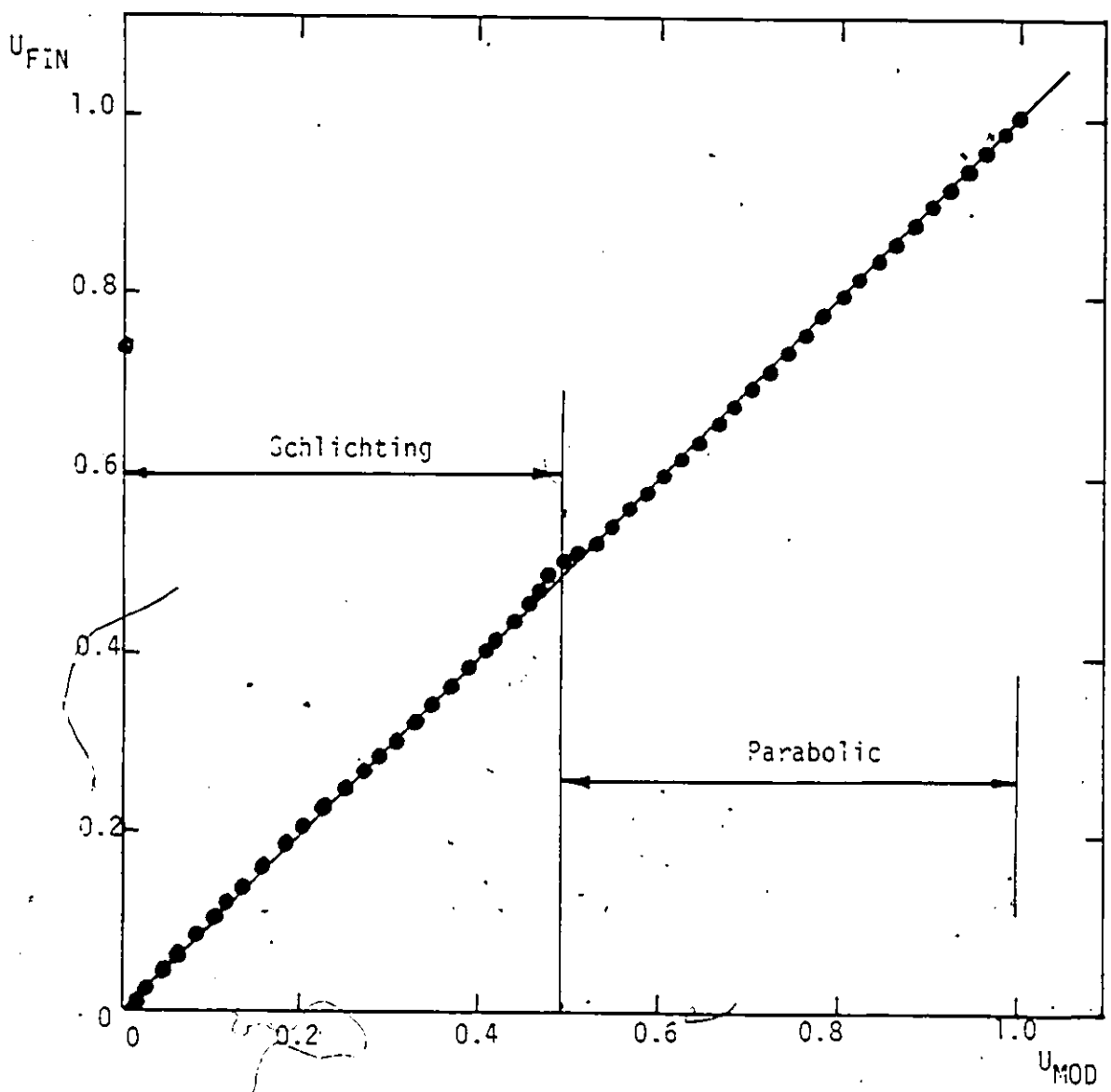


Figure 13 Comparison of Velocity Profile Model and Finite Difference Solution ( $X_c=0.008$ )

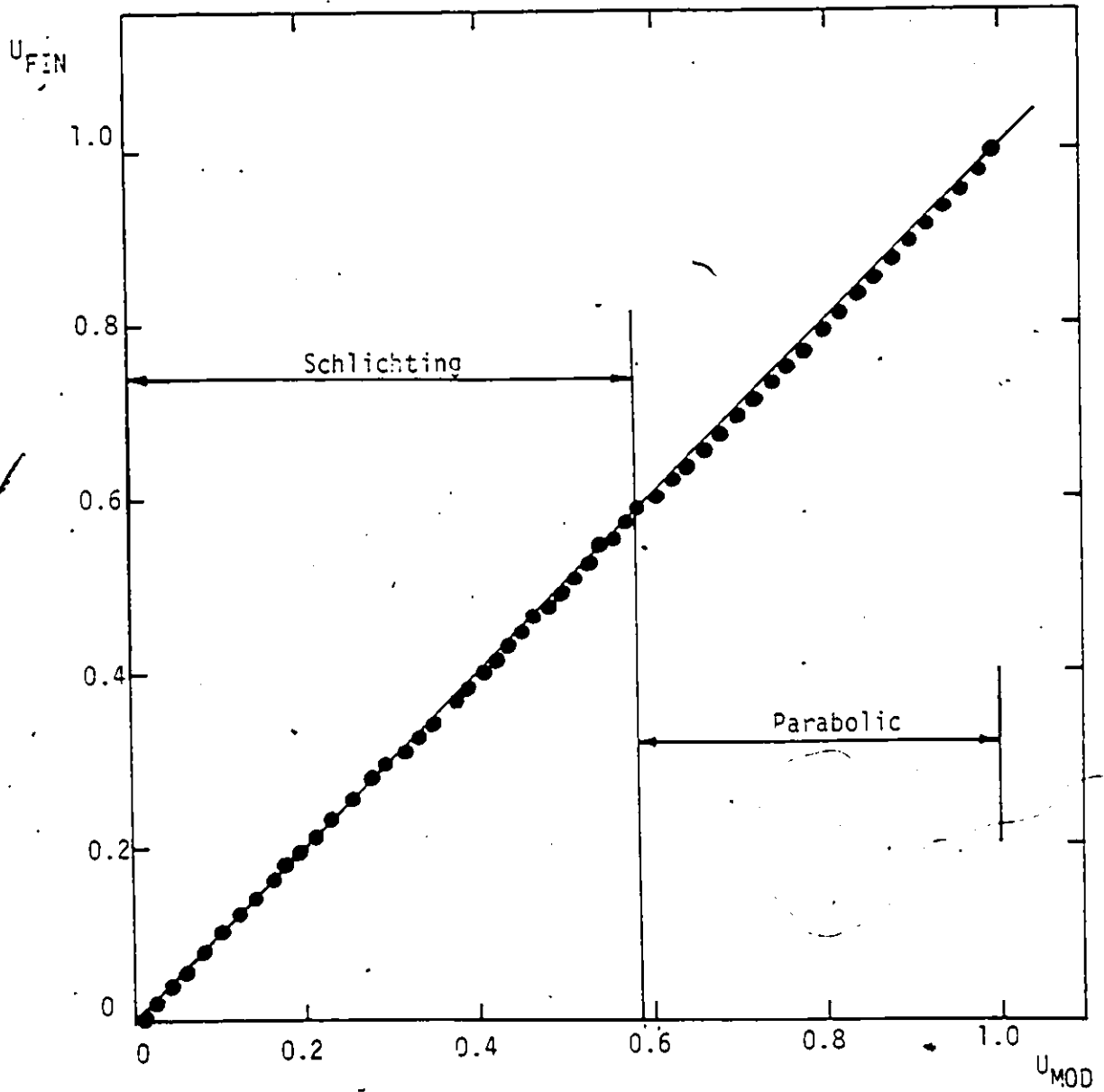


Figure 14 Comparison of Velocity Profile Model and Finite Difference Solution ( $X_c=0.016$ )

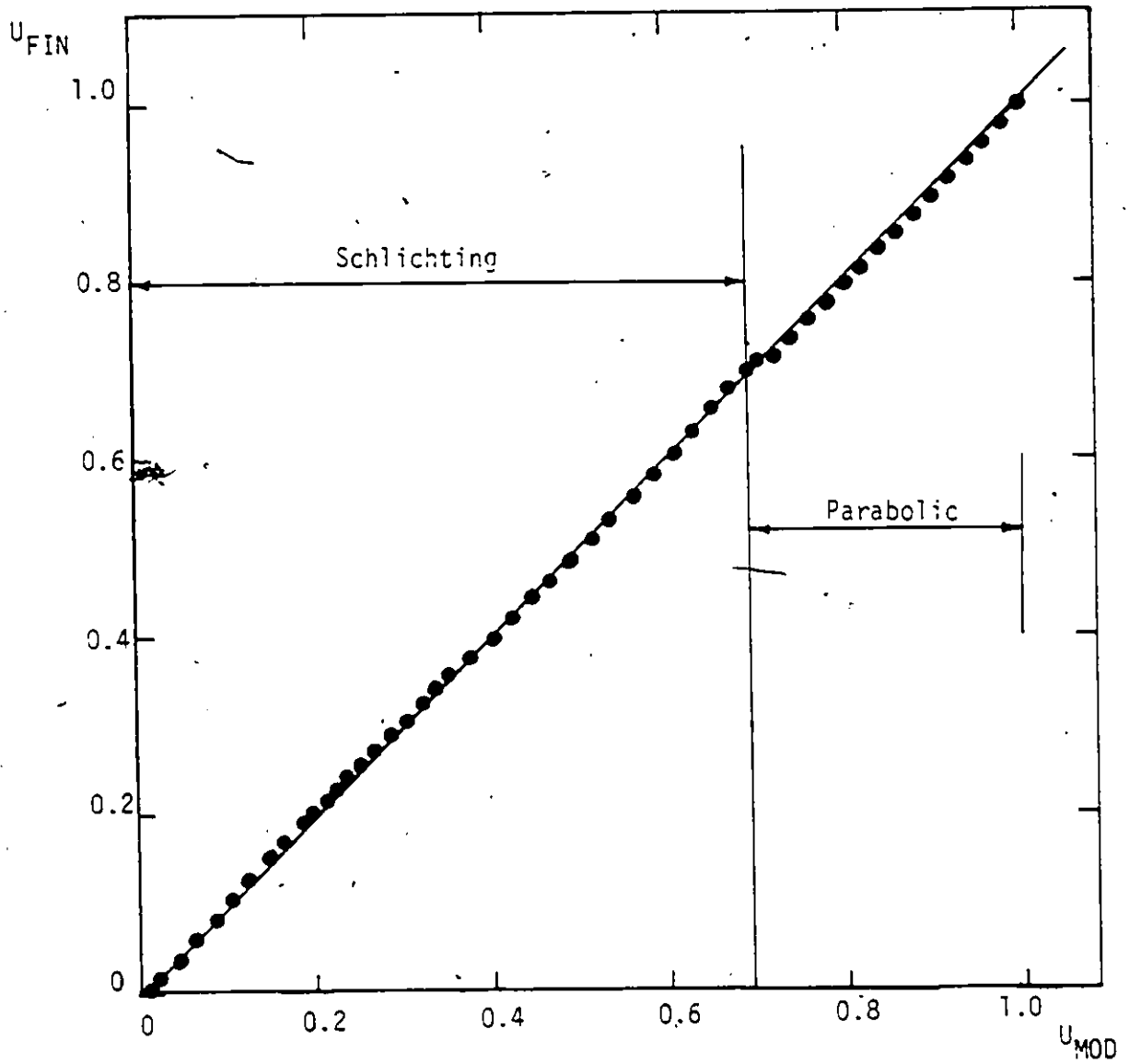


Figure 15 Comparison of Velocity Profile Model and Finite Difference Solution ( $X_c=0.028$ )



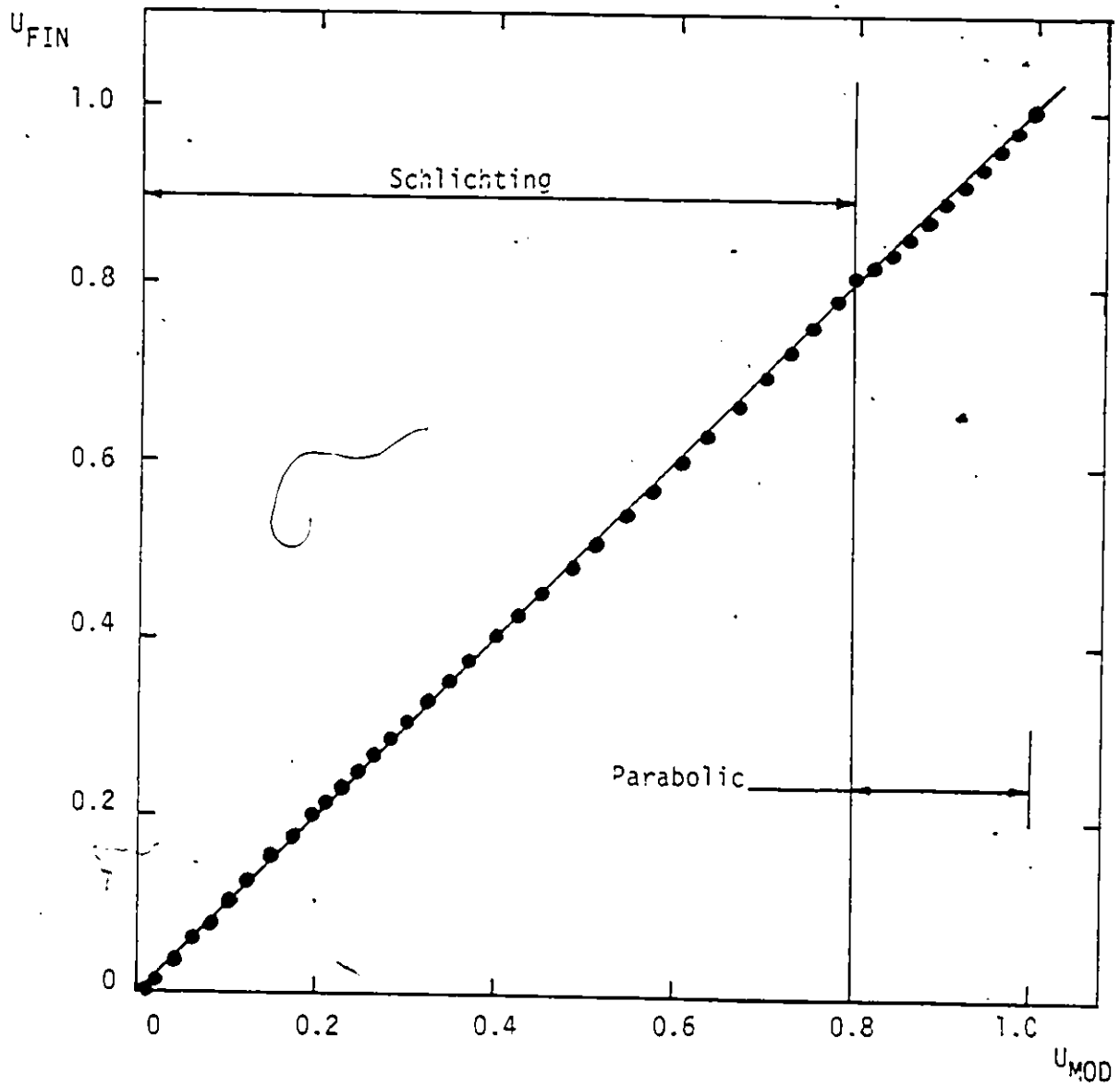


Figure 16 Comparison of Velocity Profile Model and Finite Difference Solution ( $X_c=0.04$ )

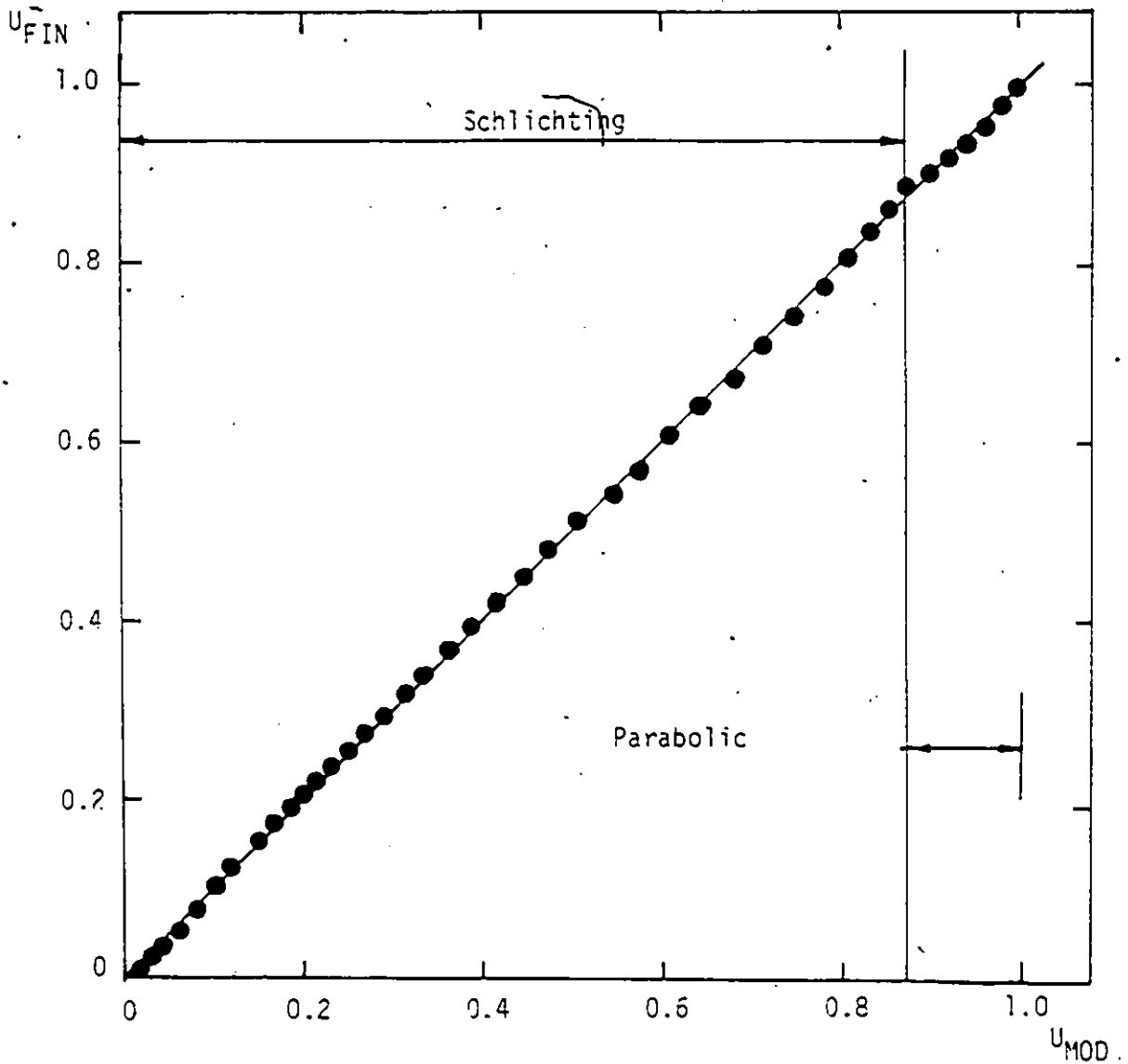


Figure 17 Comparison of Velocity Profile Model and Finite Difference Solution ( $X_c=0.048$ )

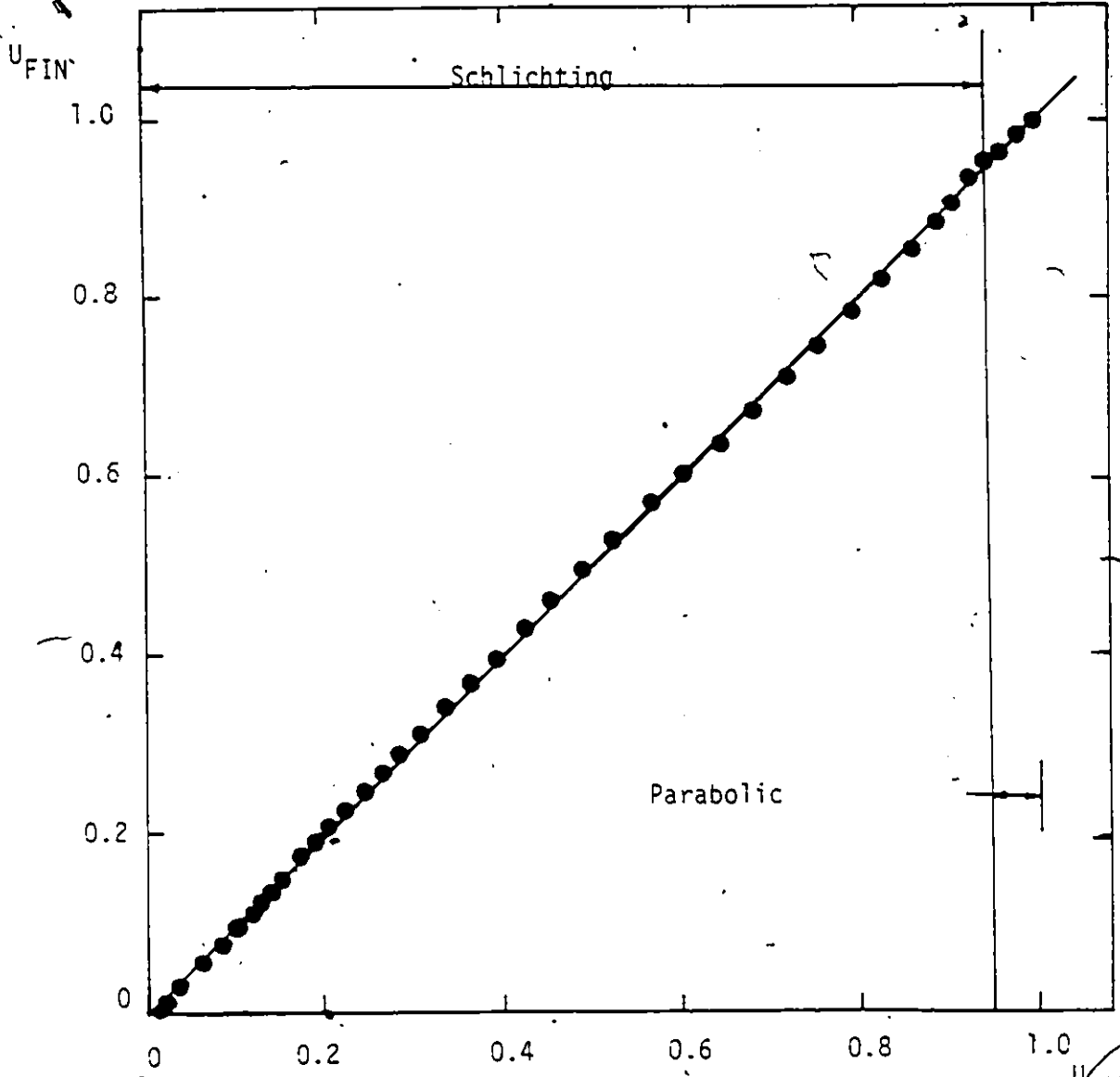


Figure 18 Comparison of Velocity Profile Model and Finite Difference Solution ( $X_c=0.056$ )

$U_{M00}$

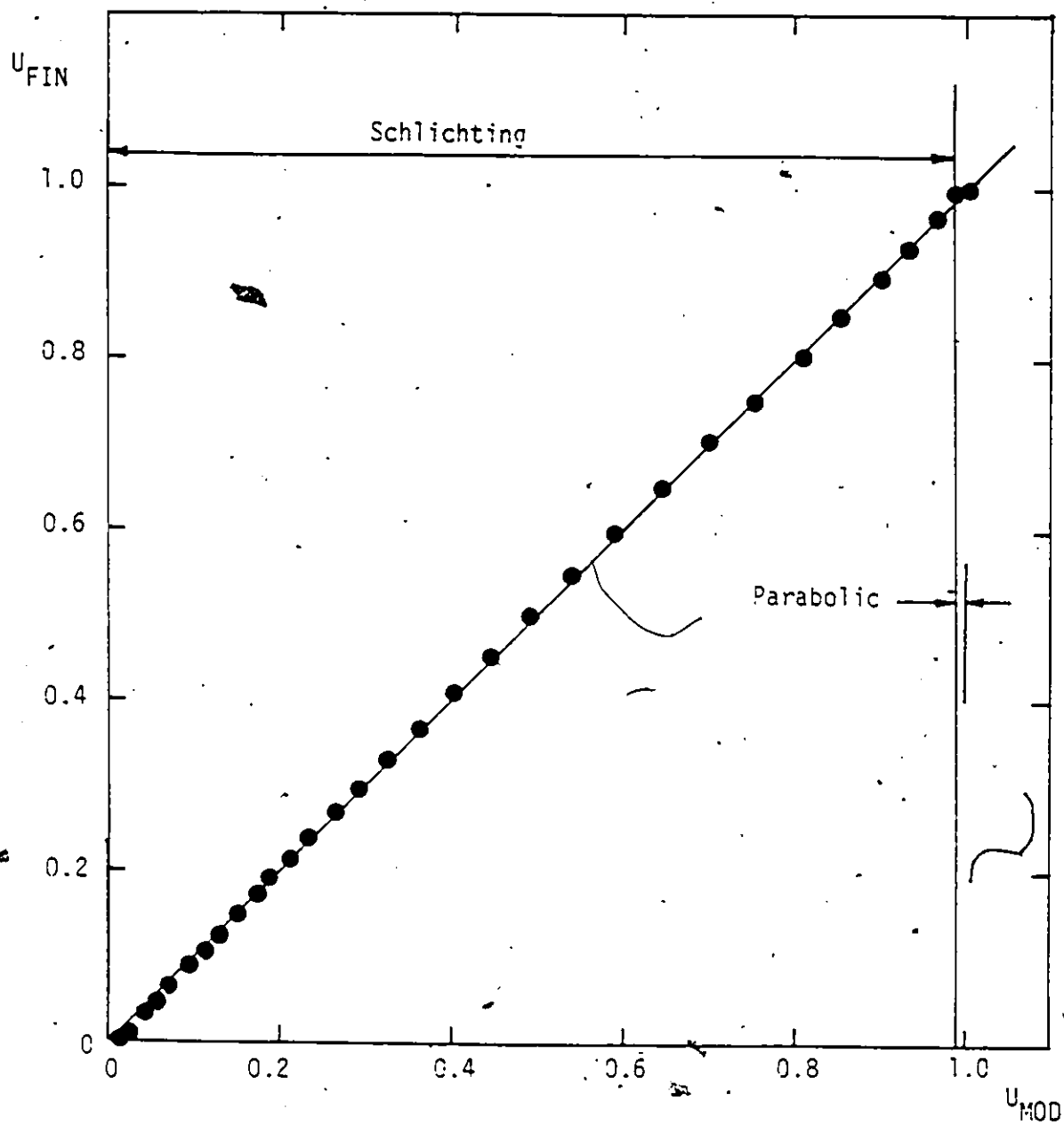


Figure 19 Comparison of Velocity Profile Model and Finite Difference Solution ( $X_c=0.1$ )

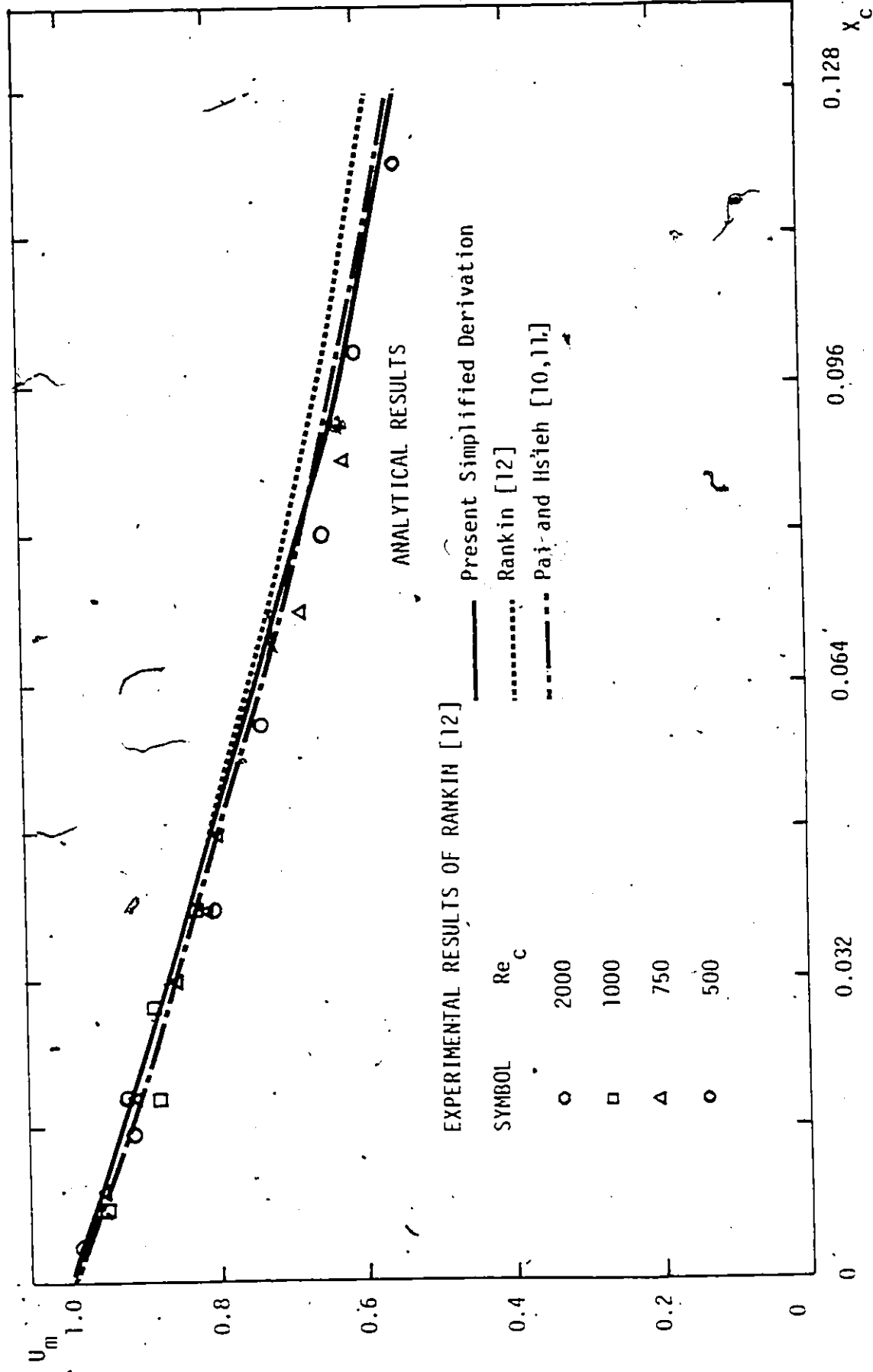


Figure 20 Maximum Velocity Decay

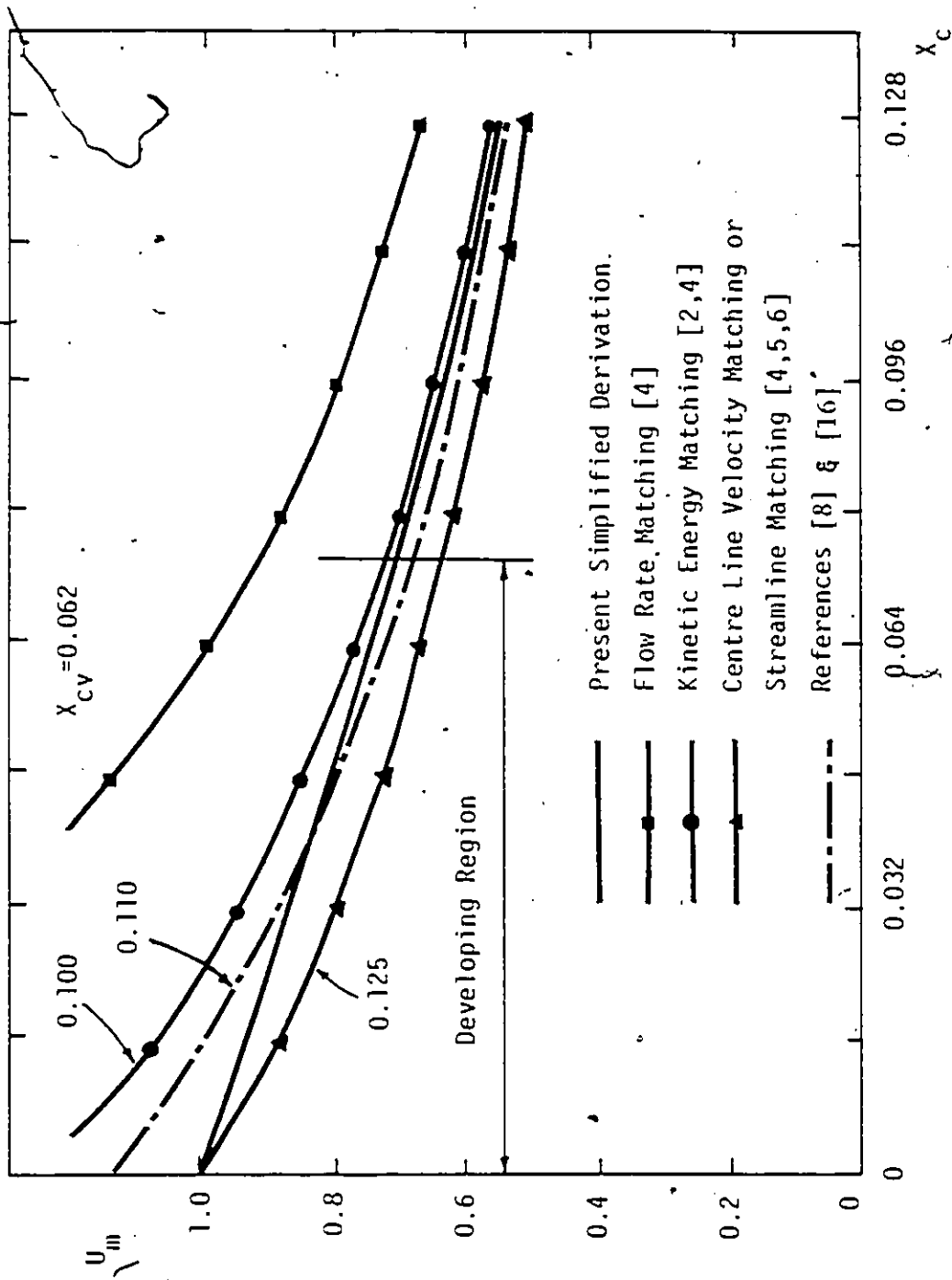


Figure 21 Comparison of Matching Schemes

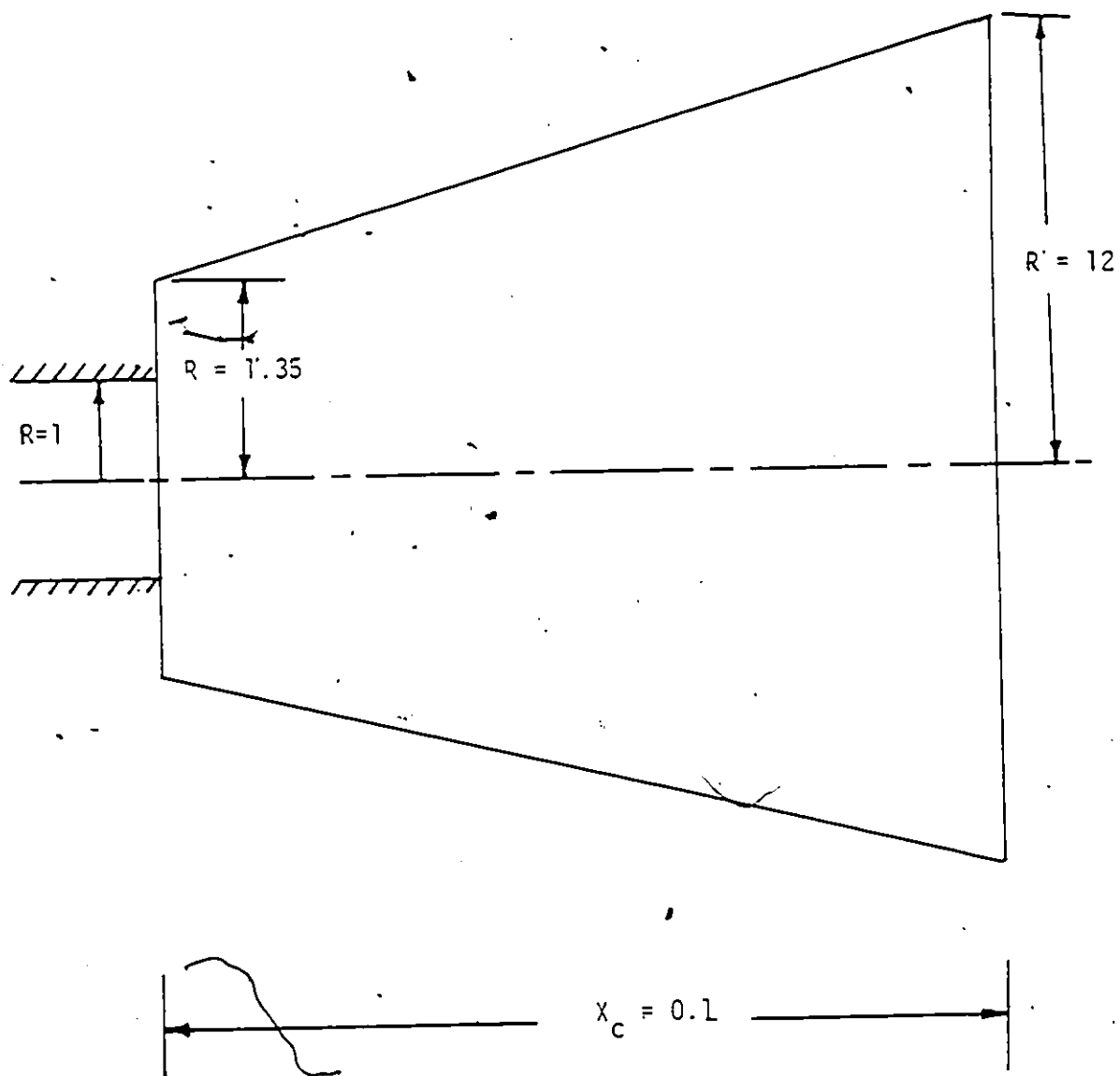


Figure 22 Solution Domain of the Jet

TABLE 1

Axial Velocity Distribution

Nondimensional Axial Velocities-U

$\frac{R}{R_m/2}$	0	.2	.4	.6	.8	1.0	1.2	1.4	1.6	1.8	2.0	2.2	2.4	2.6	2.8	3.0	3.2	3.4	3.6	3.8	4.0	$\frac{R}{R_m/2}$	$U_m$
0	1.00	0.980	0.979	0.979	0.979	0.979	0.979	0.979	0.979	0.979	0.979	0.979	0.979	0.979	0.979	0.979	0.979	0.979	0.979	0.979	0.979	0.979	1.000
0.004	1.00	0.979	0.919	0.818	0.678	0.500	0.312	0.166	0.079	0.035	0.014	0.004	0.000	0.000	0.000	0.000	0.000	0.000	0.000	0.000	0.000	0.000	0.984
0.008	1.00	0.979	0.917	0.814	0.671	0.500	0.333	0.201	0.114	0.063	0.034	0.018	0.009	0.004	0.001	0.000	0.000	0.000	0.000	0.000	0.000	0.000	0.967
0.012	1.00	0.979	0.914	0.807	0.664	0.500	0.345	0.222	0.137	0.083	0.049	0.030	0.018	0.011	0.006	0.003	0.001	0.000	0.000	0.000	0.000	0.000	0.950
0.016	1.00	0.978	0.911	0.801	0.658	0.500	0.354	0.237	0.154	0.098	0.063	0.040	0.026	0.017	0.011	0.007	0.004	0.003	0.001	0.000	0.000	0.000	0.934
0.020	1.00	0.977	0.907	0.795	0.653	0.500	0.360	0.248	0.166	0.109	0.073	0.048	0.032	0.022	0.015	0.010	0.007	0.005	0.003	0.002	0.001	0.001	0.916
0.024	1.00	0.976	0.904	0.790	0.649	0.500	0.365	0.257	0.176	0.120	0.081	0.055	0.038	0.026	0.019	0.013	0.009	0.007	0.005	0.003	0.002	0.002	0.898
0.028	1.00	0.975	0.900	0.786	0.645	0.500	0.369	0.264	0.184	0.128	0.088	0.062	0.043	0.031	0.022	0.016	0.012	0.008	0.006	0.004	0.003	0.003	0.880
0.032	1.00	0.974	0.898	0.782	0.642	0.500	0.372	0.269	0.191	0.134	0.094	0.067	0.048	0.034	0.025	0.018	0.014	0.010	0.008	0.006	0.004	0.004	0.862
0.036	1.00	0.973	0.896	0.779	0.640	0.500	0.375	0.274	0.196	0.140	0.100	0.071	0.051	0.037	0.028	0.020	0.015	0.012	0.009	0.007	0.005	0.005	0.844
0.040	1.00	0.973	0.894	0.776	0.638	0.500	0.377	0.277	0.201	0.145	0.104	0.075	0.055	0.040	0.030	0.022	0.017	0.013	0.010	0.008	0.006	0.006	0.827
0.044	1.00	0.972	0.892	0.774	0.636	0.500	0.379	0.280	0.204	0.148	0.108	0.079	0.058	0.043	0.032	0.024	0.019	0.014	0.011	0.008	0.006	0.006	0.809
0.048	1.00	0.972	0.891	0.772	0.635	0.500	0.381	0.283	0.208	0.152	0.111	0.082	0.061	0.045	0.034	0.026	0.020	0.015	0.012	0.010	0.007	0.007	0.792
0.052	1.00	0.971	0.889	0.770	0.634	0.500	0.382	0.286	0.211	0.155	0.114	0.084	0.063	0.047	0.036	0.027	0.021	0.016	0.013	0.010	0.008	0.008	0.776
0.056	1.00	0.971	0.888	0.769	0.633	0.500	0.383	0.287	0.213	0.158	0.117	0.087	0.065	0.049	0.037	0.029	0.022	0.017	0.014	0.010	0.008	0.008	0.759
0.060	1.00	0.970	0.887	0.768	0.632	0.500	0.384	0.289	0.215	0.160	0.119	0.089	0.067	0.051	0.039	0.030	0.023	0.018	0.014	0.011	0.009	0.009	0.743
0.064	1.00	0.970	0.887	0.767	0.631	0.500	0.385	0.291	0.217	0.162	0.121	0.091	0.068	0.052	0.040	0.031	0.024	0.019	0.015	0.012	0.010	0.010	0.728
0.068	1.00	0.970	0.886	0.766	0.631	0.500	0.386	0.292	0.219	0.164	0.123	0.092	0.070	0.053	0.041	0.032	0.025	0.020	0.016	0.013	0.010	0.010	0.713
0.072	1.00	0.970	0.885	0.765	0.630	0.500	0.386	0.293	0.220	0.165	0.124	0.094	0.071	0.055	0.042	0.033	0.026	0.020	0.016	0.013	0.011	0.011	0.698
0.076	1.00	0.970	0.885	0.764	0.630	0.500	0.387	0.294	0.222	0.167	0.126	0.095	0.072	0.056	0.043	0.034	0.027	0.021	0.017	0.014	0.011	0.011	0.684
0.080	1.00	0.969	0.884	0.763	0.629	0.500	0.387	0.295	0.223	0.168	0.127	0.096	0.073	0.057	0.044	0.034	0.027	0.022	0.017	0.014	0.011	0.011	0.671
0.084	1.00	0.969	0.884	0.763	0.629	0.500	0.388	0.296	0.224	0.169	0.128	0.097	0.074	0.057	0.045	0.035	0.028	0.022	0.018	0.014	0.012	0.012	0.657
0.088	1.00	0.969	0.884	0.763	0.629	0.500	0.388	0.296	0.225	0.170	0.129	0.098	0.075	0.058	0.045	0.036	0.028	0.023	0.018	0.015	0.012	0.012	0.645
0.092	1.00	0.969	0.883	0.762	0.628	0.500	0.388	0.297	0.225	0.171	0.130	0.099	0.076	0.059	0.046	0.036	0.029	0.023	0.019	0.015	0.012	0.012	0.632
0.096	1.00	0.969	0.883	0.762	0.628	0.500	0.389	0.298	0.226	0.172	0.131	0.100	0.077	0.060	0.047	0.037	0.029	0.023	0.019	0.015	0.012	0.013	0.620
0.100	1.00	0.969	0.883	0.761	0.628	0.500	0.389	0.298	0.227	0.172	0.131	0.101	0.078	0.060	0.047	0.037	0.030	0.024	0.019	0.016	0.013	0.013	0.609
SCHEMATIC	1.00	0.968	0.880	0.757	0.625	0.500	0.392	0.305	0.236	0.182	0.142	0.111	0.087	0.069	0.055	0.045	0.036	0.030	0.025	0.021	0.017	0.017	



TABLE 2

## Development Lengths and Virtual Origin Locations

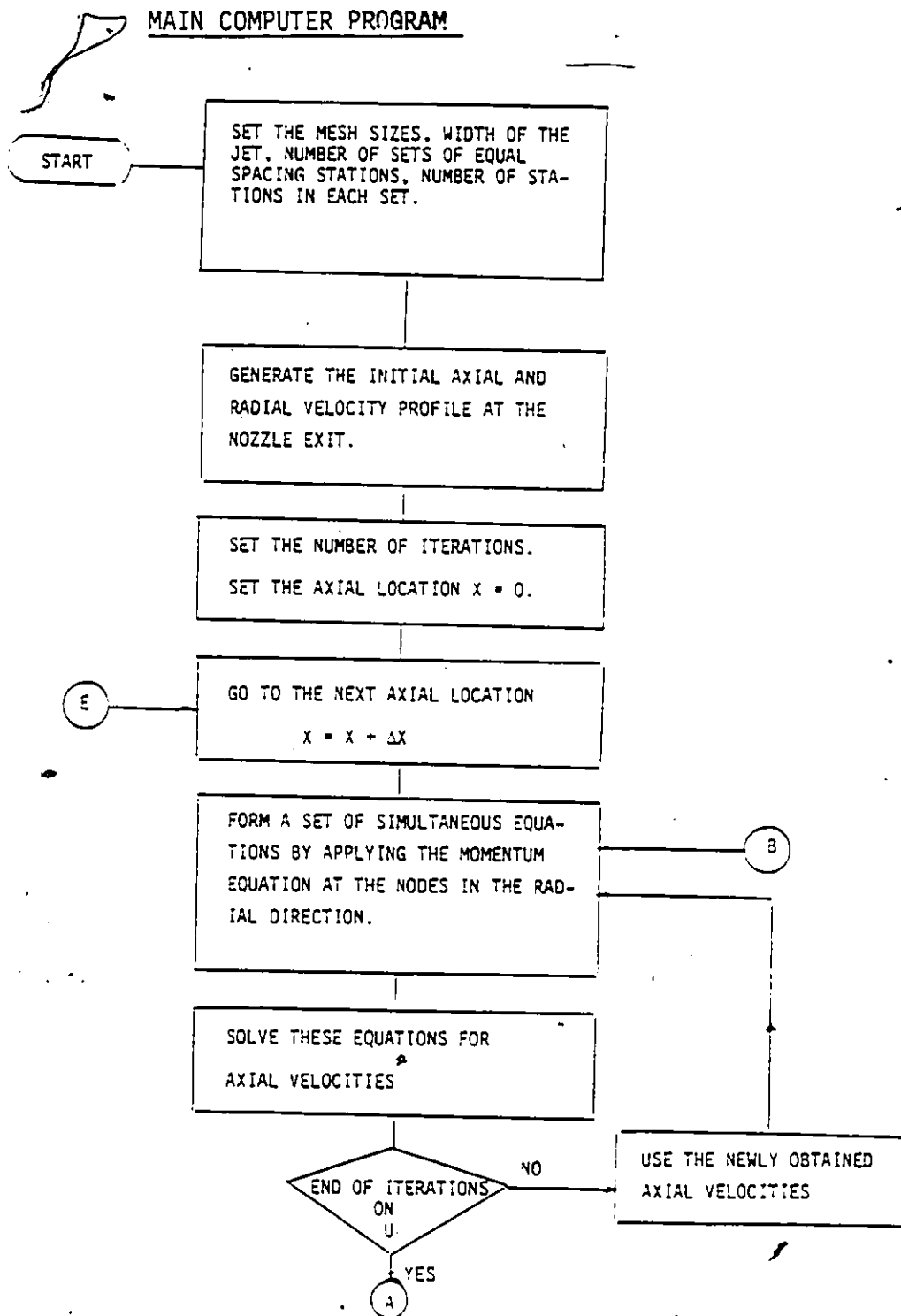
Method	References	$X_{cv}$	$X_{cl}$
Present Case: Matching $U_m$ and $dU_m/dX_c$ at $X_c = X_{cl}$	-	0.1036	0.0732
Centre Line Velocity Matching at $X_c = 0$	[4,5,6]	0.1252	-
Kinetic Energy Matching at $X_c = 0$	[2,4]	0.1	-
Flow Rate Matching at $X_c = 0$	[4]	0.0624	-
Streamline Matching at $X_c = 0$ and $r = a$	[4,5]	0.1252	-
du Plessis et al.	[8]	0.11	0.06
Tsang	[16]	0.11	0.07
Chang	[6]	0.1112	$20/Re_c$
Dmitriyev and Kulesova ( $X_{cv}$ is assumed)	[7]	0.1	0.0752

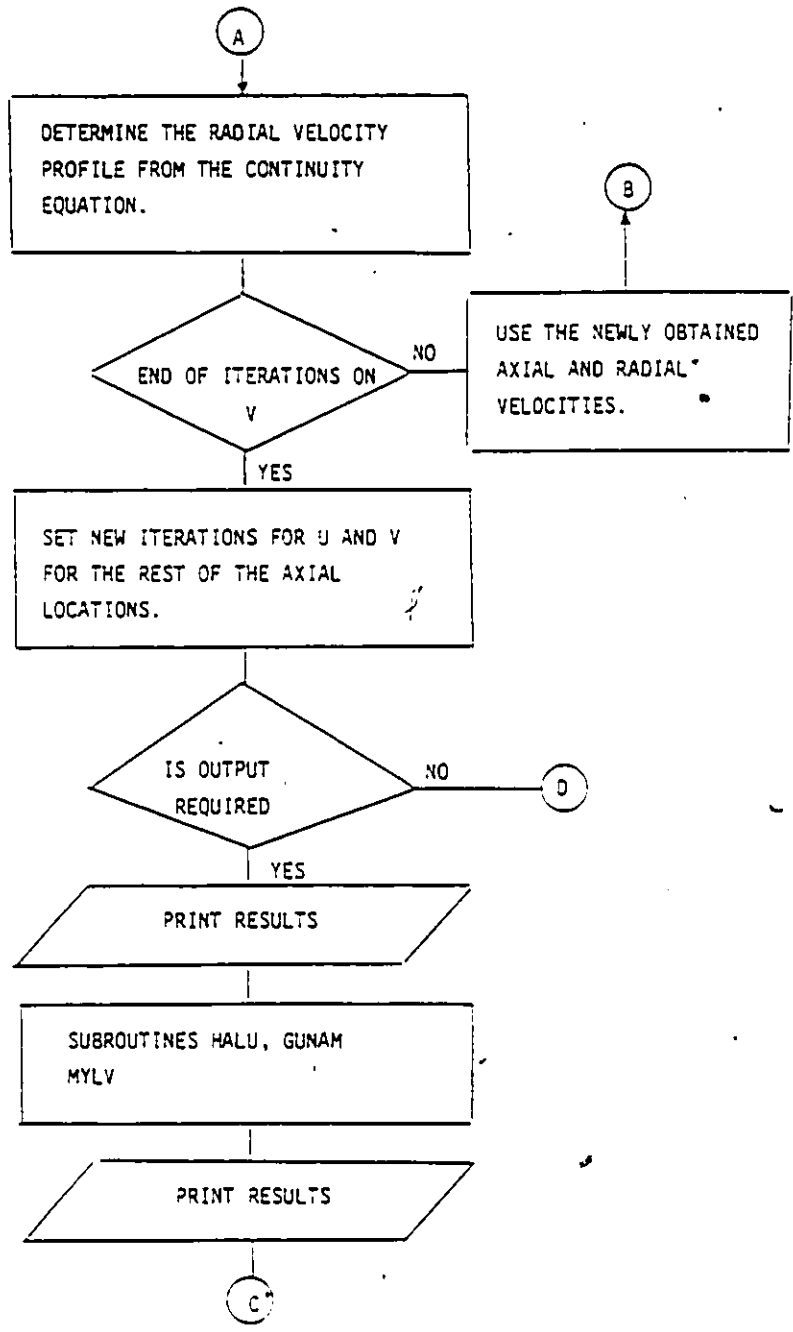
TABLE 3  
Schlichting Parameters in the Free Shear Layer

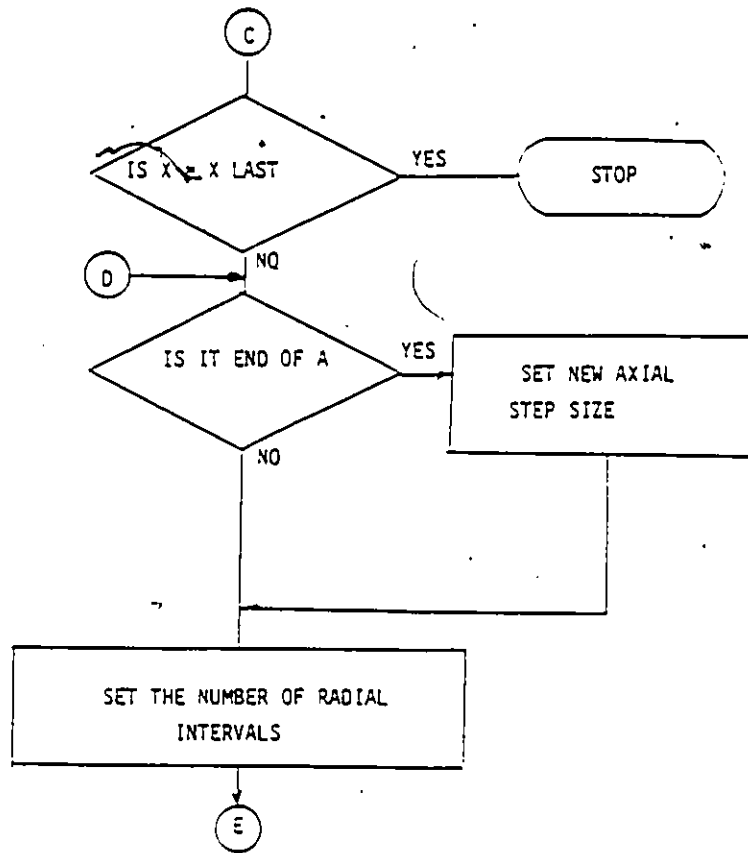
Axial Distance	The Radial Location of the Maximum Velocity of Matching Schlichting A	Spread Parameter $\gamma/Re_c$	Distance of Virtual Origin $x_{cv}$
0.001	0.7910	0.0181	0.0011
0.004	0.6832	0.0410	0.0036
0.008	0.6009	0.0630	0.0073
0.012	0.5388	0.0815	0.0113
0.016	0.4863	0.0979	0.0156
0.020	0.4402	0.1128	0.0202
0.024	0.3980	0.1267	0.0250
0.028	0.3592	0.1396	0.0299
0.032	0.3227	0.1517	0.0350
0.036	0.2876	0.1633	0.0403
0.040	0.2540	0.1743	0.0458
0.044	0.2216	0.1848	0.0515
0.048	0.1901	0.1948	0.0574
0.052	0.1595	0.2043	0.0635
0.056	0.1382	0.2127	0.0692
0.060	0.1119	0.2187	0.0736
0.064	0.1012	0.2221	0.0759
0.068	0.0872	0.2263	0.0791
0.072	0.0795	0.2297	0.0808
0.076	0.0734	0.2306	0.0822
0.080	0.0684	0.2321	0.0833
0.084	0.0639	0.2335	0.0843
0.088	0.0600	0.2347	0.0851
0.092	0.0565	0.2358	0.0859
0.096	0.0536	0.2366	0.0865
0.100	0.0508	0.2375	0.0871

## APPENDIX A

## MAIN COMPUTER PROGRAM







The Functions of the Subroutines:

1. HALU: At the axial distance specified, the subroutine is used to determine the value of  $R_{m/2}$ , the nondimensional radial location where the axial velocity is one half of that at the centre line.
2. MYLV: Used to determine  $U$  and  $R/R_{m/2}$ .
3. GUNAM: Used to determine the width of the parabolic core by comparing the finite difference solution with a parabolic profile.

Variables Used in the Program

NYL	= Total number of grid points in y direction.
NYE	= Grid point at the edge of the jet exit.
LL	= Number of sets of equally spaced stations.
LI(LL)	= Number of stations to be calculated in each set.
AHI(LL)	= Spacing between stations in each set.
N(LL)	= Total number of grid points less 1 in each set.
KY	= Number of iterations for radial velocity.
KY1	= Number of iterations on U at first station of the first set.
KY2	= Number of iterations on U in the first set.
KY3	= Number of iterations on U in the rest of the sets.
XST	= Developing length of the jet.
RM	= $\frac{R}{Rm/2}$
RMU	= U
PARU	= Magnitude of $U_0$ at the edge of the parabolic core (from finite difference solution)
BU	= Magnitude of $U_0$ at the edge of the parabolic core (from the generated parabolic velocity profile)

```

//A53SRUBA JOB (R13100R6FB,30,4), 'ARUL', CLASS=S
EXEC FORTGCLG, REGION=300K
//PORT.SYSIN DD *
REAL*8 A(1451), B(1451), C(1451), D(1451), UP(1451),
*V(1451), U(1451)
REAL*8 AM(1451), AN(1451), AU(1451), AHI(5)
REAL*8 P
DIMENSION LI(5), N(6)
COMMON U
P=.001D00
P2=P**2
NY=1450
NY1=1451
NYE=1001
NYR=1449
LL=5
LI(1)=100
LI(2)=25
LI(3)=25
LI(4)=25
LI(5)=25
AHI(1)=1.E-05
AHI(2)=1.E-05
AHI(3)=1.E-05
AHI(4)=1.E-05
AHI(5)=1.E-05
N(1)=1350
N(2)=1375
N(3)=1400
N(4)=1425
N(5)=1450
N(6)=1450
XST=.12
KY=10
KYP=10
KY1=5
KY2=5
KY3=5
KD=KYP-1
DO 51 I=1, NY1
IF (I-NYE) 501, 503, 503
501 UP(I)=1-(FLOAT(I-1)*P)**2
GO TO 51
503 UP(I)=0.
51 CONTINUE
DO 52 I=1, NY1
V(I)=0.
52 CONTINUE
X=0.
DO 9800 KL=1, LL

```



```

NY=N(KL)
NYN=N(KL+1)
NY1=NY+1
NYR=NY-1
L=LI(KL)
AH=AH(KL)
DO 9000 KKK=1,L
X=X+AH
DO 9200 K=1,KYP
DO 9100 KA=1,KY1
DO 17 I=1,NY
  IF(KA.GT.1) GOTO 202
  UCO=UP(I)
  GO TO 203
202  UCO=U(I)
203  B(I)=UCO*P2/AH+2.
      D(I)=UCO*P2/AH*UP(I)
17   CONTINUE
      B(1)=B(1)+2.
      AM(1)=B(1)
      AN(1)=-4./AM(1)
      AU(1)=D(1)/AM(1)
DO 66 I=2,NY
  AA=-(1.+(V(I)-1./(I-1)/P)*P/2.)
  CA=-1.+P/2.*(V(I)-1./(I-1)/P)
  AN(I)=B(I)-AA*AN(I-1)
  AN(I)=CA/AM(I)
  AU(I)=(D(I)-AU(I-1)*AA)/AM(I)
66  CONTINUE
  IF ((KA-KY1).LT.0) GOTO 306
DO 61 I=1,NY
  B(I)=U(I)
61  CONTINUE
306  U(NY)=AU(NY)
DO 88 J=1,NYR
  I=NY-J
  U(I)=AU(I)-AN(I)*U(I+1)
88  CONTINUE
9100 CONTINUE
DO 63 I=1,NY
  U(I)=.5*(B(I)+U(I))
63  CONTINUE
  V(1)=0.
  V(2)=-P/4./AH*(U(2)-UP(2)+U(1)-UP(1))
DO 29 M=3,NY
  V(M)=FLOAT(M-2)/FLOAT(M-1)*V(M-1)-
* .5*P/AH*(U(M)-UP(M)+
* FLOAT(M-2)/FLOAT(M-1)*(U(M-1)-UP(M-1)))
29  CONTINUE
  KY1=KY2
  IF(K.NE.KE) GO TO 9200

```

```

DO 67 I=1,NY
C(I)=V(I)
A(I)=U(I)
67 CONTINUE
9200 CONTINUE
DO 68 I=1,NY
V(I)=.5*(C(I)+V(I))
U(I)=.5*(U(I)+A(I))
68 CONTINUE
IF(KKK.NE.L)GOTO 233
91 PRINT 500,X
500 FORMAT(/,'AVERAGE VALUE FOR U,V AT X=',E15.7,/)
PRINT 400
I=1
234 IF (I.GT.NY)GOTO 235
PRINT 420,I,UP(I),U(I),V(I)
400 FORMAT(/5X,'I',4X,'UP(I)',6X,'U(I)',7X,'V(I)'/)
420 FORMAT(2X,I4,4X,F7.4,4X,F7.4,4X,F7.2)
I=I+50
GOTO 234
235 CONTINUE
PRINT 601
601 FORMAT(////)
PRINT 600,(I,U(I),V(I),I=1,NY)
600 FORMAT(2X,I7,4X,D28.16,4X,D28.16)
CALL HALU(NY,P,HALFR)
CALL MYLV(HALFR,P,NY)
CALL GUNAM(NY,P)
235 CONTINUE
235 CONTINUE
DO 65 I=1,NY
UP(I)=U(I)
65 CONTINUE
DO 110 M=NY1,NYN
UP(M)=0.
110 CONTINUE
69 IF(X.LT.XST)GOTO 9000
KYP=KY
9000 CONTINUE
KY1=KY3
KY2=KY3
9800 CONTINUE
STOP
END
SUBROUTINE HALU(NY,P,HALFR)
COMMON U
REAL*8 U(1451)
HALFU=U(1)/2.
DO 10 I=1,NY
IF(U(I).NE.HALFU)GOTO 20
HALFR=P*FLOAT(I-1)

```

```

      GO TO 13
20  IF (U(I).LT.HALFU)GOTO 14
10  CONTINUE
14  HALFR=(HALFU-U(I-1))/(U(I)-U(I-1))
      *      *(P*FLOAT(I-1)+P*FLOAT(I-2))
      *      +P*FLOAT(I-2)
13  PRINT 100
      PRINT 200,HALFR,HALFU
100  FORMAT(7/75X,HALFR,5X,HALFU)
200  FORMAT(2X,F7.4,3X,F7.4)
      RETURN
      END
      SUBROUTINE MYLU(HALFR,P,NY)
      COMMON U
      REAL*8 U(1451)
      DIMENSION TR(1451)
100  PRINT100
      FORMAT(7/7)
125  PRINT125
      FORMAT(3X,RM,10X,RMU)
      DO 10 I=1,NY
          TR(I)=P*FLOAT(I-1)/HALFR
10  CONTINUE
      RM=0.
      DO 30 J=1,19
          DO 30 I=J,NY
              IF (RM.GT.TR(I))GOTO 30
              IF (RM.LE.TR(I))GOTO 200
              RMU=(U(I)-U(I-1))/(TR(I)-TR(I-1))
              *      (RM-TR(I-1))/(U(I-1)-U(I))
              RMU=RMU/RMU
              GOTO 300
30  CONTINUE
200  RMU=U(I)/U(I)
300  PRINT 300,RM,RMU
300  FORMAT(2X,F7.4,5X,F7.4)
      RM=RM+.1
20  CONTINUE
      RETURN
      END
      SUBROUTINE GUNAM(NY,P)
      COMMON U
      REAL*8 U(1451)
      I=1
      PARU=1.
      U CALL NORMALISED VALUE (OF U(I)) AS BU
      BU=1.
300  IF (BU-PARU.LE.0.001)GOTO 400
      I=I+1
      PARU=1.-(P*FLOAT(I-1)+P)**2
      BU=U(I)/U(I)

```

```
GOTO 800
500 PRINT 1000,I,PARU,BU
1000 FORMAT(/7X,'I=',I4,4X,'PARU=',F7.4,5X,'BU=',F7.4)
RETURN
END

/*
//GO.SYSIN DD *
//
```

```
GOTO 800 -  
900 PRINT 1000, I, PARU, BU  
1000 FORMAT(/7X, 'I=', I4, 4X, 'PARU=', F7.4, 5X, 'BU=', F7.4)  
RETURN  
END
```

```
/*  
//GO.SYSIN DD *  
//
```

SAMPLE OUTPUT

LINE DISTANCE 40#0 001

LINE	DISTANCE	VALUE	UNIT
1	0.0000000000000000	00	
2	0.0000000000000000	00	
3	0.0000000000000000	00	
4	0.0000000000000000	00	
5	0.0000000000000000	00	
6	0.0000000000000000	00	
7	0.0000000000000000	00	
8	0.0000000000000000	00	
9	0.0000000000000000	00	
10	0.0000000000000000	00	
11	0.0000000000000000	00	
12	0.0000000000000000	00	
13	0.0000000000000000	00	
14	0.0000000000000000	00	
15	0.0000000000000000	00	
16	0.0000000000000000	00	
17	0.0000000000000000	00	
18	0.0000000000000000	00	
19	0.0000000000000000	00	
20	0.0000000000000000	00	
21	0.0000000000000000	00	
22	0.0000000000000000	00	
23	0.0000000000000000	00	
24	0.0000000000000000	00	
25	0.0000000000000000	00	
26	0.0000000000000000	00	
27	0.0000000000000000	00	
28	0.0000000000000000	00	
29	0.0000000000000000	00	
30	0.0000000000000000	00	
31	0.0000000000000000	00	
32	0.0000000000000000	00	
33	0.0000000000000000	00	
34	0.0000000000000000	00	
35	0.0000000000000000	00	
36	0.0000000000000000	00	
37	0.0000000000000000	00	
38	0.0000000000000000	00	
39	0.0000000000000000	00	
40	0.0000000000000000	00	
41	0.0000000000000000	00	
42	0.0000000000000000	00	
43	0.0000000000000000	00	
44	0.0000000000000000	00	
45	0.0000000000000000	00	
46	0.0000000000000000	00	
47	0.0000000000000000	00	
48	0.0000000000000000	00	
49	0.0000000000000000	00	
50	0.0000000000000000	00	
51	0.0000000000000000	00	
52	0.0000000000000000	00	
53	0.0000000000000000	00	
54	0.0000000000000000	00	
55	0.0000000000000000	00	
56	0.0000000000000000	00	
57	0.0000000000000000	00	
58	0.0000000000000000	00	
59	0.0000000000000000	00	
60	0.0000000000000000	00	
61	0.0000000000000000	00	
62	0.0000000000000000	00	
63	0.0000000000000000	00	
64	0.0000000000000000	00	
65	0.0000000000000000	00	
66	0.0000000000000000	00	
67	0.0000000000000000	00	
68	0.0000000000000000	00	
69	0.0000000000000000	00	
70	0.0000000000000000	00	
71	0.0000000000000000	00	
72	0.0000000000000000	00	
73	0.0000000000000000	00	
74	0.0000000000000000	00	
75	0.0000000000000000	00	
76	0.0000000000000000	00	
77	0.0000000000000000	00	
78	0.0000000000000000	00	
79	0.0000000000000000	00	
80	0.0000000000000000	00	
81	0.0000000000000000	00	
82	0.0000000000000000	00	
83	0.0000000000000000	00	
84	0.0000000000000000	00	
85	0.0000000000000000	00	
86	0.0000000000000000	00	
87	0.0000000000000000	00	
88	0.0000000000000000	00	
89	0.0000000000000000	00	
90	0.0000000000000000	00	
91	0.0000000000000000	00	
92	0.0000000000000000	00	
93	0.0000000000000000	00	
94	0.0000000000000000	00	
95	0.0000000000000000	00	
96	0.0000000000000000	00	
97	0.0000000000000000	00	
98	0.0000000000000000	00	
99	0.0000000000000000	00	
100	0.0000000000000000	00	

IN	AM
0.0000	1.5000
0.1000	0.9950
0.2000	0.9900
0.3000	0.9850
0.4000	0.9799
0.5000	0.9749
0.6000	0.9698
0.7000	0.9648
0.8000	0.9597
0.9000	0.9547
1.0000	0.9500
1.1000	0.9460
1.2000	0.9419
1.3000	0.9380
1.4000	0.9337
1.5000	0.9294
1.6000	0.9252
1.7000	0.9211
1.8000	0.9171

1=199

2=200=0.3632

3U=0.3643

### Program Description

The program is written in FORTRAN IV for an IBM 3031 computer and needs approximately 550 K memory. The variables used in the program are given in Appendix A.

Figure 22 shows the solution domain of the jet considered in the present computational work. The program determines the velocity distribution up to the axial distance  $X_c = 0.1$ . The entire flow field is divided into a number of sets  $LL(I)$ . Each of these sets consists of a number of stations  $LI(I)$ . The stations are equally spaced. The distance between two consecutive stations in a set, the axial step size, is denoted by  $AHI(I)$ . Up to the axial length of 0.068 the radial step size of 0.001 is used while from  $X_c = 0.068$  to  $X_c = 0.1$  the radial step size is set at 0.002. The number of grid points in the radial direction at each axial station is denoted by  $N(I)$  and determined by the radial width at that particular axial station.

The description of the calculation at the  $j+1$ th station when the velocity distributions at the  $j$ th station is known is given below.

If the nozzle exit is considered as the  $j$ th station the axial velocity distribution is known to be parabolic while the radial velocity distribution is zero. These axial velocities are stored in arrays  $UP(I)$  and  $V(I)$ . During the first iteration on the axial velocity at the  $j+1$ th station the coefficients of the  $(N-1)$  simultaneous equations are formed by substituting the values of  $UP(N)$  and  $V(N)$  in the equation (3.10). The program then solves these equations for the axial velocities at the station  $j+1$ .  $(N-1)$  simultaneous equations at  $j+1$ th



station are again formed where the coefficients of these equations are now obtained by using the new axial velocities. These equations are again solved for U. The process of forming (N-1) simultaneous equations repeatedly by using the newly calculated axial velocities is controlled by the number of iterations specified on U (i.e. KY1). Then the program calculates the radial velocities from the continuity equation. The program then returns to the point where it begins the calculation of U. Since the loop which calculates U is nested inside the V loop the axial velocities are iterated KY1\*KYP times where KYP is the number of iterations on V. Then the program calculates the  $R_{m/2}$ ,  $\frac{U_0}{U_m}$  and  $\frac{R}{R_{M/2}}$  and the extent of the parabolic region  $R_p$  from the subroutines HALU, MYLV and GUNAM respectively. Once the solution at the  $j+1$  the station is found the program goes to the next station by considering the present station as the  $j$ th station.

Due to computing time restrictions, obtaining the solution to the whole flow field in a single run of the computer was not feasible. This problem was circumvented by storing the output at an intermediate location on a tape and reading them as input for the  $j$ th station to continue the computation.

APPENDIX B  
UNCERTAINTY ANALYSIS

The parabolic velocity profile is given by the equation:

$$U_o = U_m(1-R^2) \quad (B.1)$$

When the axial velocity is normalized with the local centre line velocity, equation (B.1) can be rewritten in the following form:

$$\frac{u}{u_m} = (1-R^2) \quad (B.2)$$

(i.e.) 
$$U = 1 - R^2 \quad (B.3)$$

The uncertainty of  $U$  is given by the following equation:

$$w_U = \left[ \left( \frac{\partial U}{\partial R} \cdot w_R \right)^2 \right]^{1/2} \quad (B.4)$$

From equation (B.3);

$$\frac{\partial U}{\partial R} = -2R \quad (B.5)$$

The smallest radial step size used in the finite difference calculation is 0.001, hence, the uncertainty on  $R$  is chosen as 0.0005.

Therefore,

$$w_U = 0.001R.$$

APPENDIX C

NLIN COMPUTER PROGRAM

```

JOB (R13100R6FB,10,12),ARULRASA,CLASS#A
EXEC SAS,REGION=LION
*BIN ID *
DATA ARUL;
INPUT I U;
LABEL U=VELOCITY
I=POSITION;
CARDS;
PROC PRINT N;
TITLE ACTUAL DATA;
PROC NLIN;
PARMS A=0 TO 1. BY 1;
B=0 TO .005 BY .001;
C=0.000001 TO .2 BY .01;
MODEL U=I*(A+B*I**2+C*I**3);
DER.H=I*(2*B*I+C*3*I**2);
DER.B=I*(2*B*I**2+C*3*I**3);
DER.C=I*(2*B*I**3+C*3*I**4);
OUTPUT OUT=NEW;
PREDICTED=UNEW;
PROC PLOT DATA=NEW;
PLOT UNEW*1-P* UNEW*A UNEW*B;

```

SAMPLE OUTPUT AT XCE0.002  
 ACTUAL DATA 12:24 THURSDAY, FEBRUARY 25, 1982 26

NON-LINEAR LEAST SQUARES SUMMARY STATISTICS  
 DEPENDENT VARIABLE: U

SOURCE	DF	SUM OF SQUARES	MEAN SQUARE
REGRESSION	3	2.17940416	0.72646805
RESIDUAL	106	0.00200945	0.00001895
UNCORRECTED TOTAL	109	2.18141362	
(CORRECTED TOTAL)	108	1.18149524	

PARAMETER	ESTIMATE	ASYMPTOTIC STD. ERROR	ASYMPTOTIC 95% CONFIDENCE INTERVAL	
			LOWER	UPPER
A	0.74334658	0.00440517	0.73451284	0.75218031
B	0.00073883	0.00003487	0.00066765	0.00081000
C	0.00391630	0.00012777	0.00366950	0.00417297

ASYMPTOTIC CORRELATION MATRIX OF THE PARAMETERS

	A	B	C
A	1.000000	-0.790708	-0.778300
B	-0.790708	1.000000	0.170333
C	-0.778300	0.170333	1.000000

APPENDIX DADDITIONAL MODIFICATION IN PAI AND HSIEH'S  
COMPUTER PROGRAM

The computer program given in reference [10] is for a two dimensional jet with rectangular initial velocity distribution. In the case of an axisymmetric jet, the changes necessary in this program are also given by them. However, it is noticed that in addition to the given changes, the statement  $AM(1) = -2./AM(1)$  should be changed to  $AN(1) = -4./AM(1)$  when an axisymmetric jet is considered.

VITA AUCTORIS

1950

Born in Negombo, Sri Lanka on December 22

1973

Completed National Diploma in Technology at Hardy  
Senior Technical Institute, Amparai, Sri Lanka

1978

Received the Degree of Bachelor of Mechanical Engineering  
from the Kingston Polytechnic, Kingston-Upon-Thames,  
Surrey, England

1982

Candidate for the Degree of Master of Applied Science  
at the University of Windsor, Windsor, Ontario, Canada.